Thesis for the degree of Licentiate of Engineering

Power loss minimization in electric cars by wheel force allocation

JULIETTE TORINSSON

Department of Mechanics and Maritime Sciences
CHALMERS UNIVERSITY OF TECHNOLOGY
Göteborg, Sweden 2020

Power loss minimization in electric cars by wheel force allocation
JULIETTE TORINSSON

THESIS FOR LICENTIATE OF ENGINEERING no 2020:17

Department of Mechanics and Maritime Sciences
Chalmers University of Technology
SE–412 96 Göteborg
Sweden
Telephone: +46 (0)31–772 1000

Cover:
Polar bear in a snow storm.

Chalmers Digitaltryck
Göteborg, Sweden 2020

"I'll just go down and have some pudding and wait for it all to turn up... It always does in the end."
-Luna Lovegood

Power loss minimization in electric cars by wheel force allocation

Juliette Torinsson
Department of Mechanics and Maritime Sciences
Chalmers University of Technology

Abstract

The need for lowering the emission levels has never been greater than now. In the vehicle industry, electrification seems to be an irreversible way ahead but user-related challenges such as limited range delay electricity as the primary energy source for personal transportation. Other control-related challenges are also introduced as electric cars are over-actuated, i.e. several actuators can be used for the same purpose. Over-actuation introduces the possibility to choose more freely which actuator to use when. Can this freedom of choice be used to improve energy efficiency of electric cars by e.g. minimizing power losses? In this thesis, two wheel force distribution algorithms have been developed with a method called control allocation. The algorithms minimize power losses in the electric drivetrain, transmission and tires. They were tested in a simulated city cycle in a Volvo V60 configuration with four electric motors, each connected to a wheel through a single speed transmission and coupling respectively. It was found that by using developed algorithms, up to 3.9% energy could be saved. In a next step, the transmission ratio on the front motors and rear motors were optimized in combination with one of the algorithms. By using a larger transmission ratio in the front than in the rear, the energy consumption reduced even further. With these development steps, up to 7.9% energy could be saved compared to the original vehicle.

Keywords: energy efficiency, electric vehicles, control allocation.

Acknowledgements

The work presented in this thesis would not have been possible without the guidance of a number of people, contributing on so many levels, both work-related and personal. I want to start by extending my gratitude to Fyrklövern, my excellent supervision trio. First, I want to thank my main supervisor, Dr. Mats Jonasson, for his endless support, encouraging counsel and interesting discussions on work-related topics as well as fishing and bread making. I want to thank Dr. Derong Yang for her valuable insights from the industry and her contagious positive attitude. Last but not least, I want to extend my gratitude to Prof. Bengt Jacobson, for his seemingly infinite knowledge and valuable input to the project.

I am also grateful for my colleagues at Chalmers and Volvo Cars, for the enjoyable working environment and interesting conversations around the coffee table. A special thanks to Sonja for always being helpful and supportive, and for contributing with such warmth to the VEAS division, and to Anders Peterson, for giving me the opportunity to work with this interesting and rewarding project.

Thank you, Mamma and Pappa, my brothers Max and Leonard, my bonus dad Lennart, and Busan, Elsa and Nisse, for providing me with such loving support that I could not have succeeded without. I also want to extend my gratitude to my dear friends, old and new. Hanna and Emma, thank you for keeping an eye on me, catching me before I realize that I am falling. Sina, Randi, Magnus and Johannes, thank you for showing me such comradery and teamwork in an otherwise lonesome profession. Finally, I want to thank my beloved husband Daniel for being a solid rock, keeping me grounded, and such a goofball, taking my mind off my troubles by always making me laugh.

List of included papers

This thesis consists of the following papers. References to the papers will be made using Roman numerals.

I. Torinsson, J., Jonasson, M., Yang, D., and Jacobson, B., *Energy reduction by power loss minimisation through wheel torque allocation in electric vehicles: a simulation-based approach.* Accepted for publication in Vehicle System Dynamics.

II. Torinsson, J., Jonasson, M., Yang, D., and Jacobson, B., *A study on transmission ratios and power loss minimization in electric vehicles.* Extended abstract to be submitted to IAVSD 2021.

The following publications are relevant for the topic but not included in the thesis.

III. Torinsson, J., Jonasson, M., Yang, D., and Jacobson, B., *An energy efficient method to control electric propulsive system in a vehicle.* Patent application no. 20164034.9-1202, 2020.

IV. Torinsson, J., *A study to distribute wheel torque to increase energy efficiency for electric vehicles.* Energirelaterad Transportforskning 2020, Energimyndigheten.

Table of Contents

Chapter 1

Introduction and motivation

The need for lowering the emission levels has never been greater than now. Electrification seems to be an irreversible way ahead. The increased level of electrification, with electric motors as faster and more precise actuators, introduces new opportunities compared to vehicles equipped with the internal combustion engine. However, user-related challenges such as limited range, long charging times and the limited power grid network for charging stations are delaying electricity as the primary energy source of personal transportation. It is, thus, important to continuously improve energy efficiency of electric vehicles.

1.1 Problem motivating this research

Apart from aforementioned challenges, control-related challenges are introduced with electric vehicles that have not been presented in petrol or diesel vehicles. In contrast to petrol and diesel engine driven vehicles, where there has typically been one driveline for each vehicle, electric propulsion demands vehicle engineering to broaden the spectrum and work with several powertrains per vehicle. An increased number of electric motors contributes to *over-actuation* which was previously seen mainly in aircraft and marine vessels [1]. Over-actuation means that the motion request from the driver can be attained in several different ways using different actuators. If a vehicle with four electric motors, one for each wheel, is driven and the electric mo-

tors could be used for both propulsion and regenerative braking, there is an infinite number of torque distributions that would fulfill the forward motion requested by the driver. If a yawing request is added, e.g. from steering wheel, even more solutions appear as yaw motion can be achieved either through different propulsive or brake torques on left and right side, or steering of the wheels.

With the increasing over-actuation of electric vehicles, the ability to choose between several actuators opens up new abilities to improve energy efficiency. During a braking scenario in an electric vehicle, for example, both friction brakes and the electric motors can be used for deceleration. The electric motors, however, will extend the range of the battery due to regenerative braking. Through the choice of actuators, one can choose to use the one which is less energy expensive to fulfill desired request. Considering an electric vehicle with two different electric motors, one can find combinations of operation of the motors that uses the least amount of power. This *choice* or *coordination* of actuators can be solved through a method called *control allocation*.

The coordination of actuators, in this thesis, is momentaneous as opposed to predictive. Predictive methods such as energy saving cruise controllers and automation of steering are used to reduce energy consumption. These systems, which are already employed in the market, look ahead and plan the operation of the vehicle accordingly. In [2, 3], for example, offline speed profile optimization and model predictive control is used to minimize the energy consumption for heavy vehicles. Using offline planning or predictive control, the energy consumed over a certain future driving horizon is minimized. In contrast, energy efficient momentaneous control minimizes power losses as opposed to energy consumption at every time instant. Here, power is defined as the amount of energy converted or transmitted per unit time. We can differ between useful and lost power depending on that vehicles have a transport purpose: useful power is one that moves the vehicle and lost power is the remaining e.g. iron and copper in the electric motor or hysteresis in the rubber of the tires. Hence, the total energy consumed can be reduced by minimizing the power losses momentaneously. It is expected that a higher-level control of optimal speed or acceleration requests will include the predictive aspect for energy efficiency.

Furthermore, the transmission ratio in electric vehicles is usually chosen as a trade-off between maximum speed and maximum torque. If the electric motor is connected to the wheel, the wheel torque will be the motor torque multiplied by the transmission ratio, and the wheel speed will be the motor speed divided by the transmission ratio according to:

$$\tau_w = n\tau_m \qquad\qquad \omega_w = \frac{\omega_m}{n}$$

Too high transmission ratio will enable high maximum wheel torque but limit the maximum speed of the vehicle due to the maximum rotational speed of the motor. If the transmission ratio is low, the vehicle can reach higher velocities at the cost of lower maximum wheel torque. Assuming that there are at least one motor on the front axle and one of the rear axle and that these can be decoupled from the wheel, then one way of facilitating this trade-off between maximum torque and maximum speed is to have different transmission ratios front and rear.

1.2 Research questions

The following questions are hereby investigated in this thesis:

I. How to allocate individual wheel, including axle-wise, drive and brake torques to minimize power losses, and at the same time follow the driver intentions on vehicle motion?

II. In a vehicle with at least one electric machine on each axle, how can different transmission ratios front and rear be used to reduce energy consumption?

1.3 Limitations

This thesis deals with momentaneous control of wheel forces rather than predictive control. Path planning such as adapting speed according to topology of surrounding environment is left to either a human driver or automated driving algorithm. Furthermore, the energy required for auxiliary devices

such as air conditioning, sound system, cooling of motors etc. is not included in this work. Instead, the power losses in the powertrain components, batteries and tires are in focus in present thesis.

1.4 Contributions

This thesis contributes to:

- Exploring intuitive offline and online optimization schemes for the reduction of energy consumption for everyday driving.
- Investigating how varying the transmission ratios of motors on front and rear axle affects energy consumption.
- Developing a simulation environment with power loss models for electric motors and inverters, tires and transmission and implementing them in optimization.

The thesis is structured in the following way. In chapter 2 a method of controlling over-actuated systems called control allocation is defined. In chapter 3, the methodology used in present work is described including the simulation environment, control architecture, the development of the control allocation algorithms, the modeled power losses as well as validation of these. In chapter 4, the results from the wheel force optimization and transmission ratio investigation is presented and discussed. Finally, in chapter 5, the conclusions of this work are presented and future outlook explored.

Chapter 2

Control Allocation

Historically, vehicles were equipped with actuators that each had a specific purpose; the internal combustion engine was used to propel the vehicle, friction brakes were used to brake the vehicle, etc. As research and implementation regarding e.g. safety increases, the actuators now have more uses. For example, the friction brakes are now used in electronic stability control and active rollover protection. Furthermore, with the introduction of electric motors in e.g. hybrid electric vehicles, there is another actuator which can both propel and brake the vehicle. The system is redundant in the sense that it has several actuators that can perform the same task. How to coordinate actuator requests can be solved with control allocation. Control allocation is a method that solves an underdetermined system of equations, that decides which actuator to use for a specific request in a system with redundant actuators. This chapter will introduce the control allocation problem and various ways of solving it. Then, a brief literature review of how this method's application to the momentaneous power loss optimization, and how to handle actuator saturation and actuator dynamics is discussed.

2.1 Definition of over-actuation

There is an underlying assumption when a decision is to be made for which actuator to use for a specific purpose; the possibility to *choose*. The freedom of choice is a consequence of the system being *over-actuated*, i.e. there are less degrees of freedom to control than there are actuators which can control

them. For example, the electric motors in an electric vehicle cannot only be used to accelerate the vehicle but also to decelerate it. Deceleration is mainly controlled by friction brakes but, in electric vehicles, there is an opportunity to use either of the actuators. The degree of freedom to control is longitudinal (braking), i.e. 1, and the number of actuators that can control it is 2; friction brakes and electric motors. Hence, the system is over-actuated; there is a redundant number of actuators.

2.2 Definition of control allocation

Control allocation is an approach to solve the control problem concerning over-actuated systems, by distributing the total control demand among several actuators [4]. In control allocation, the actuator selection task is separated from the regulation task in the control design. In the regulation task, the total control effort to produce is specified but not how to produce it. Through this separation, the choice of actuator can be optimized for the considered application. Another benefit is that actuator saturation can be taken into account and the remainder of the control effort can be redistributed to another unsaturated actuator. Furthermore, the same control law can be used for several different hardware configurations with different actuators which can reduce development cost in a car manufacturer OEM that produces a number of different car models.

A general definition given by [4] defines a control allocator mathematically to solve an underdetermined and typically constrained, system of equations. Consider the following dynamic system. Here, we do not consider the constraints yet, i.e. no inequality $\mathbf{h}(\mathbf{x}, \mathbf{g}) < 0$.

$$\dot{\mathbf{x}} = \mathbf{f}(\mathbf{x}, \mathbf{g}(\mathbf{u})) \tag{2.1}$$

where the derivatives $\dot{\mathbf{x}}$ of the states,i.e. the motion to be controlled, can be expressed as a function of the states $\mathbf{x}$ and system input $\mathbf{u}$. Here, the assumption is made that the dynamic system (2.1) is separable according to:

$$\dot{\mathbf{x}} = \mathbf{f}(\mathbf{x}) + \mathbf{g}(\mathbf{u}) \tag{2.2}$$

Assuming that a certain input $\mathbf{u}^*$ provides the desired motion $\dot{\mathbf{x}}_{\text{des}}$, (2.2) can be rearranged into,

$$\mathbf{g}(\mathbf{u}^*) = \dot{\mathbf{x}}_{\text{des}} - \mathbf{f}(\mathbf{x}) \tag{2.3}$$

where $\mathbf{u}^*$ is determined by the control allocator.

The input to the control allocator is the requested control effect known as the virtual control input, $\mathbf{v}$ (the right hand side of equation (2.3)). The output of the control allocator is the requests to the actuators, $\mathbf{u}$. Given $\mathbf{v}$, $\mathbf{u}$ is sought such that

$$\mathbf{v} = \mathbf{g}(\mathbf{u}) \tag{2.4}$$

where $\mathbf{g}$ is the mapping from the true control input to the virtual input in the system to be controlled. The regulation design can then be determined by,

$$\dot{\mathbf{x}} = \mathbf{f}(\mathbf{x}) + \mathbf{v} \tag{2.5}$$

The linear case is almost exclusively studied where the relationship between virtual control input and the requests to the actuator is linearized. Linearizing equation (2.4) around $\mathbf{u}_0$ gives us,

$$\mathbf{v} = \mathbf{g}(\mathbf{u}_0) + \frac{\partial \mathbf{g}}{\partial \mathbf{u}}(\mathbf{u}_0) \cdot (\mathbf{u} - \mathbf{u}_0) \tag{2.6}$$

The standard linear control allocation problem is then defined as,

$$\bar{\mathbf{v}} = \mathbf{B}\mathbf{u} \tag{2.7}$$

where

$$\mathbf{B} = \mathbf{g}'(\mathbf{u}_0), \qquad \bar{\mathbf{v}} = \mathbf{v} - \mathbf{g}(\mathbf{u}_0) + \mathbf{B} \cdot \mathbf{u}_0 \tag{2.8}$$

$\bar{\mathbf{v}} \in \mathbb{R}^{k \times 1}$, $\mathbf{u} \in \mathbb{R}^{m \times 1}$, $\mathbf{B} \in \mathbb{R}^{k \times m}$ where $\mathbf{B}$ is called the control effectiveness matrix. In the case of $m = k$, i.e. the matrix $\mathbf{B}$ is square and assuming it is invertible the solution $\mathbf{u}^*$ can be found by simply inverting $\mathbf{B}$ in (2.7).

$$\mathbf{u}^* = \mathbf{B}^{-1}\bar{\mathbf{v}} \tag{2.9}$$

If, however, $m > k$ and matrix $\mathbf{B}$ has rank k it is not invertible and, therefore, there are no unique solutions to the system of equations (2.7). Hence, a function or a method to find the inverse mapping based on matrix $\mathbf{B}$ is sought. This, according to [5], is defined as control allocation.

There are different methods of control allocation, e.g. pseudo-inverse, daisy-chaining and direct allocation methods. These will be introduced briefly in section 2.4 where actuator saturation is discussed. In this thesis, the focus is on one approach called optimization based control allocation [4, 6, 7] which is described further in the following section.

2.3 Optimization based control allocation

Optimization based control allocation provides the opportunity to add a secondary objective to the control allocation problem. Equation (2.10) is referred to as l_p-optimal control allocation where the weighted error is minimized.

$$\mathbf{u} = \arg\left(\min_{\mathbf{u}\in\mathbb{U}}\left(\left\|\mathbf{W}_{\mathrm{u}}(\mathbf{u}-\mathbf{u}_{\mathrm{d}})\right\|_p + \gamma\left\|\mathbf{W}_{\mathrm{v}}(\mathbf{B}\mathbf{u}-\mathbf{v})\right\|_p\right)\right) \tag{2.10}$$

where $\mathbf{u}_{\mathrm{d}}$ is the desired control input, $\mathbf{W}_{\mathrm{u}}$ and $\mathbf{W}_{\mathrm{v}}$ are weighting matrices, γ is a weighting factor and $\mathbf{u} \in \mathbb{U}$ is the space of attainable actuator requests. The optimization problem (2.10) is most frequently solved using the l_2-norm, i.e. a quadratic program [4]. The constrained quadratic program is solved using e.g. the interior point method, active set method or fix-point method. By disregarding the constraints on the actuators, i.e. releasing the requirement that $\mathbf{u} \in \mathbb{U}$, any request to the actuators $\mathbf{u}$ can fulfill $\mathbf{B}\mathbf{u} = \mathbf{v}$, and hence the optimization problem (2.10) changes to:

$$\begin{aligned} \min_{\mathbf{u}} \quad & \left\|\mathbf{W}_{\mathrm{u}}(\mathbf{u}-\mathbf{u}_{\mathrm{d}})\right\|_2 \\ \text{subject to} \quad & \mathbf{B}\mathbf{u} = \mathbf{v} \end{aligned} \tag{2.11}$$

which has the closed form solution

$$\mathbf{u} = (\mathbf{I} - \mathbf{W}_{\mathrm{u}}^{-1}(\mathbf{B}\mathbf{W}_{\mathrm{u}}^{-1})^{\dagger}\mathbf{B})\mathbf{u}_{\mathrm{d}} + \mathbf{W}_{\mathrm{u}}^{-1}(\mathbf{B}\mathbf{W}_{u}^{-1})^{\dagger}\mathbf{v} \tag{2.12}$$

where † is the pseudo-inverse operator, denoting $A^{\dagger} = A^T(AA^T)^{-1}$ as the pseudo-inverse of A. The desired control input $\mathbf{u}_{\mathrm{d}}$ is used to guide the actual control input $\mathbf{u}$ to a specific solution. It can be set to zero in order to minimize the control effort $\mathbf{u}^T\mathbf{u}$, e.g. if the power losses increase proportionally with control effort and are the same for all actuators, or if wear is to be minimized by using each actuator equally (assuming wear is proportional to control effort). It can also be used to direct the solution towards the use of a specific actuators. The desired control input $\mathbf{u}_{\mathrm{d}}$ is found prior to the control allocation. In [8] for example, $\mathbf{u}_{\mathrm{d}}$ is based on state-of-charge (SOC) and power demand in a vehicle with fuel cells, internal combustion engine and an electric motor. If all the actuators are weighted equally (i.e. $\mathbf{W}_{\mathrm{u}}$ is an identity matrix) and any $\mathbf{u}$ is possible, then one can find $\mathbf{u}_{\mathrm{d}}$ through optimization, based on some objective, e.g. to reduce power losses, and in the control allocation problem let $\mathbf{u} = \mathbf{u}_{\mathrm{d}}$.

Various authors have investigated the possibility to reduce energy consumption in over-actuated electric vehicles through control allocation of wheel torque with the objective to minimize power losses. A common approach is to use a formulation of power losses as the cost function of the optimization problem, solve it offline, and then create a mapping of how actuators should be coordinated over vehicle operating conditions which is then implemented in simulation or in a vehicle. The cost function consists of either the electric motor efficiency map [9, 10] or a polynomial curve fit of experimentally acquired power loss data of the complete electric drivetrain and tires [11, 12].

The authors in [12] explore the use of an analytical solution to the optimization problem and compares it to using distribution rules acquired through offline optimization. In [13, 14], the control allocation problem is solved online through an active-set algorithm. Online optimization methods might, however, be harder to implement in a vehicle due to increased complexity compared to an analytical solution or distribution rules.

In this work, two variants of optimization based control allocation have been developed. One variant is an online optimization problem in the form of a quadratic program where the solution is provided analytically through matrix operations. The other variant is a brute force offline optimization resulting in a lookup table which can be used online. Both methods include the ability to decouple the motors which has not yet been well covered in

literature. These variants are described further in section 3.4.

2.4 Actuator saturation and dynamics

Actuators often have limits that need to be taken into consideration. If the control allocator distributes control signals to a saturated actuator, the virtual control input may not be fulfilled. For example, electric motors has a maximum power limit that they cannot exceed. If the electric motor were to be saturated in a braking scenario, the control allocator needs to be aware of this. Otherwise the deceleration request may not be fulfilled which can have fatal outcomes.

There are many ways to handle actuator saturation summarized by [4, 6] listed below.

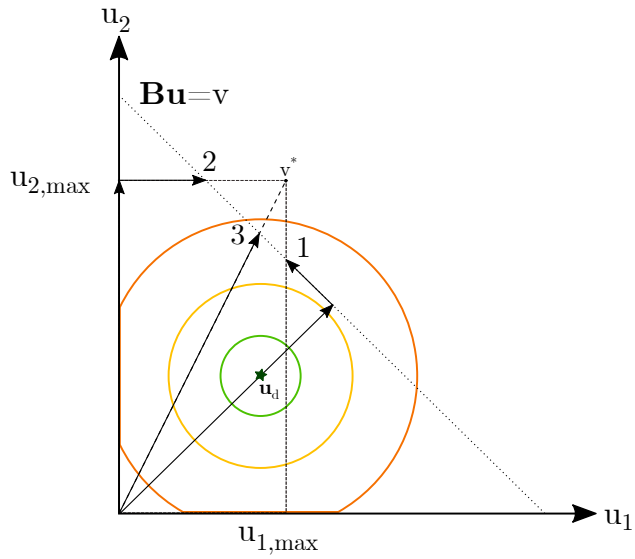

Figure 2.1: *Different methods of handling actuator saturation for a single virtual input, v, with two control variables, u_1 and u_2. The circles represents increasing optimality where the green circle is most optimal in this case with $\mathbf{u}_d$ as the desired solution. 1: Redistributed pseudo-inverse, 2: Daisy-chaining, 3: Direct allocation.*

2.4.1 Redistributed pseudo-inverse

In the redistributed pseudo-inverse method, the unconstrained control allocation problem (2.7) is solved using a pseudo-inverse method, resulting in the optimal vector $\mathbf{u} \in \mathbb{U}$ where $\mathbb{U}$ is the feasible set of control inputs. If none of the actuators are saturated, no further action is needed. If there is saturation of one or more actuators, the optimal vector $\mathbf{u}$ is projected onto the feasible set $\bar{\mathbf{u}} = \text{Proj}_{\mathbb{U}}(\mathbf{u})$. Then, the unsaturated actuators, i.e. the unsaturated elements of the control vector $\bar{\mathbf{u}}$, are recomputed in order to reduce the gap between the virtual control input and the actual input. This is visualized in figure 2.1, case 1.

2.4.2 Daisy Chaining

Daisy chaining divides the actuators into groups which are prioritized so that the group with highest priority is used first to solve the control allocation problem. If one or more actuators of the first group is saturated, the control distributed to that group is set and the remaining virtual control is allocated by the second group. This is repeated until a feasible solution is found. In figure 2.1, this is represented by case 2. In this example, actuator u_2 is in the first group. It is used until it is saturated, and then the second group, u_1, is used to allocate the remaining part of the virtual control.

2.4.3 Direct allocation

In direct control allocation, the direction of the virtual control input is preserved if there is no feasible solution. A feasible control input $\mathbf{u}^*$ is found that generates a virtual control input $\mathrm{v}^* = \mathbf{B}\mathbf{u}^*$ ($\mathbf{B} = (1, 1)$) that is of maximum magnitude in the direction of v. This is visualized in figure 2.1, case 3. The virtual control input that maximizes v^* is found and is then truncated to generate v.

2.4.4 Optimization-based methods

In optimization-based control allocation problems, the saturation limits of the actuators can be included in the optimization problem. The saturation limits may be constant or dependent on the environment. For example, in a vehicle, the wheel force is not only limited by the maximum available wheel

torque but also by the available friction force. In rainy conditions, the maximum wheel force is significantly less than during dry conditions. The normal load could also be increased due to external weight added to the vehicle (luggage or number of occupants) which also changes the available friction force. In online optimization, this environment or external dependencies can be incorporated in the actuator limits. In offline optimization, however, which is the most dominant approach in literature mentioned above, this is not as straight forward. There would need to be several dimensions of the resulting distribution rules concerning different road conditions (e.g. dry tarmac, wet, ice etc) and different normal loads. Therefore, the control input to the actuators is limited downstream after the control allocation has taken place with specific rules on how to redistribute the control input in order to fulfill the virtual control request. This is applicable as long as the dimension of the virtual control input $\mathbf{v}$ is small and the number of actuators low.

2.4.5 Actuator dynamics

The dynamics of an actuator may also play a significant role in the distribution of control signals. A vehicle with a combination of actuators such as a hybrid vehicle with fast electric motors and a relatively slow internal combustion engine need to take the dynamics of the engine into account. Otherwise, the delay in output from the engine may cause a vehicle response which initially does not match the desired motion.

Neglecting the actuator dynamics is a common assumption and works as long as the closed loop system is substantially slower than the actuator [4]. Since the actuators in this work are electric motors, and the closed loop system is the vehicle dynamics in combination with a driver that has a reaction time, the dynamics of the electric motors can be neglected. One example where the dynamics cannot be neglected is wheel slip control, e.g. in ABS- and traction control.

Chapter 3

Methodology

This chapter introduces the many different elements of the methodology as presented in 3.1. The simulation environment including the vehicle model and the drive cycle is described in section 3.1. The structure of the different function blocks in figure 3.1 is referred to as the control architecture. The conventional control architecture in a modern day vehicle is modified from the historical one-actuator-one-task approach and is not suitable for over-actuated systems such as the electric vehicle considered in this thesis. A different approach is needed which is described in section 3.2. The reference generator translates driver input to $\boldsymbol{v}_{req}$ which are here assumed to be planar vehicle force and torque requests used in the control allocator. This is described in section 3.3. The control allocator coordinates the actuator input requests based on the driver's desired motion and the most energy efficient solution. The motion fulfillment, power loss models and optimization procedures are presented in section 3.4. Finally, the validation of the power loss models used in the optimization is described in section 3.5.

3.1 Simulation Environment & Use Case

Energy consumption can be evaluated in many different driving situations which could be more or less relevant for the everyday driver. For example, energy can be minimized in an extreme maneuver with great results but will not benefit the energy consumption in any, for user or society, important way as this maneuver seldom occurs. Thus, a simulation environment with a

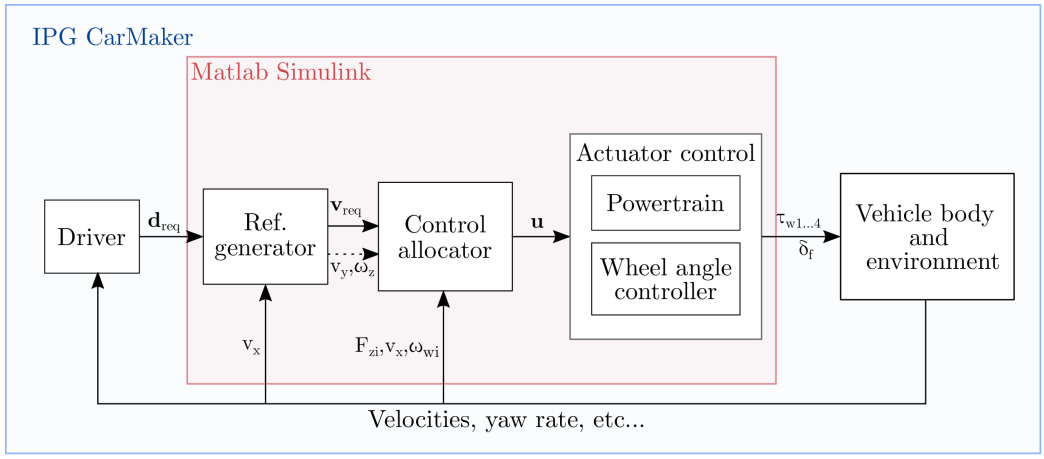

Figure 3.1: *Simulation model, control architecture and software interfaces.*

realistic surrounding environment (including aerodynamic drag, road grade, vehicle dynamics etc.), a moderate driver model and a drive cycle representing everyday driving is needed. The simulation environment is developed in IPG CarMaker and Matlab Simulink. IPG CarMaker contains the surrounding environment such as the road, the driver model and the major part of the vehicle model, i.e. the blocks in the outer box in figure 3.1. Everything in the inner box; the reference generator, control allocator and actuator control is modeled in Matlab Simulink. In this section the vehicle model will be presented first, followed by the driving scenario including the chosen drive cycle and driver model.

3.1.1 Vehicle model

The vehicle used in this thesis is a Volvo V60 configuration with four permanent magnet synchronous machines connected to each wheel respectively through a transmission and a coupling. The longitudinal motion, both propulsion and braking, is controlled completely by the electric motors, i.e. there is 100% regenerative braking. In Paper I the driver is in control of the steering, while in paper II the control allocator distributes the wheel angles. The vehicle parameters are presented in table 3.1.

The vehicle is partially modeled in IPG CarMaker, and partly in Matlab Simulink. The powertrain including the battery, the four electric motors, in-

Table 3.1: *Vehicle parameters used in Papers I and II.*

Notation	Value	Description
m	1988 kg	Vehicle total mass
I_{zz}	4300 kg/m^3	Yaw moment of inertia around CoG
l_f	1.258 m	Distance from front axle to CoG
l_r	1.615 m	Distance from rear axle to CoG
C_{yf}	93900 N/rad	Cornering stiffness for one tire on front axle
C_{yr}	84460 N/rad	Cornering stiffness for one tire on rear axle
C_{xf}	235000 N	Longitudinal stiffness for one tire on front axle
C_{xr}	180600 N	Longitudinal stiffness for one tire on rear axle
w	1.6 m	Vehicle track width
n	10 (Paper I)	Transmission ratio
η_{bat}	0.95	Round-trip efficiency of battery
η_{gb}	0.97 (Paper I)	Transmission efficiency
r_{steer}	16	Steering ratio

verters and transmission is modeled separately in Simulink. In Paper II the steering is also modeled in Simulink. The resulting wheel angles and torques are sent through external signals to IPG CarMaker where the remainder of the vehicle and the vehicle dynamics are modeled.

The energy consumption is evaluated through equation (3.1).

$$E = \int_{t_0}^{t_f} P_{tot}\, dt \tag{3.1}$$

where E is the energy consumed from start time t_0 to end time t_f, and P_{tot} is the total power defined according to (3.2). The power flow of the powetrain including the tires can be seen in figure 3.2. The total power that is evaluated here origins from the battery where positive power is defined as flow from battery towards wheel. It is assumed that the electric motors can supply any possible propulsion and brake torque in this drive cycle, hence no friction brakes are included.

$$P_{tot} = \begin{cases} \sqrt{\eta_{bat}} P_{bat}, & \text{if } P_{bat} \leq 0 \\ \frac{P_{bat}}{\sqrt{\eta_{bat}}}, & \text{if } P_{bat} > 0 \end{cases} \tag{3.2}$$

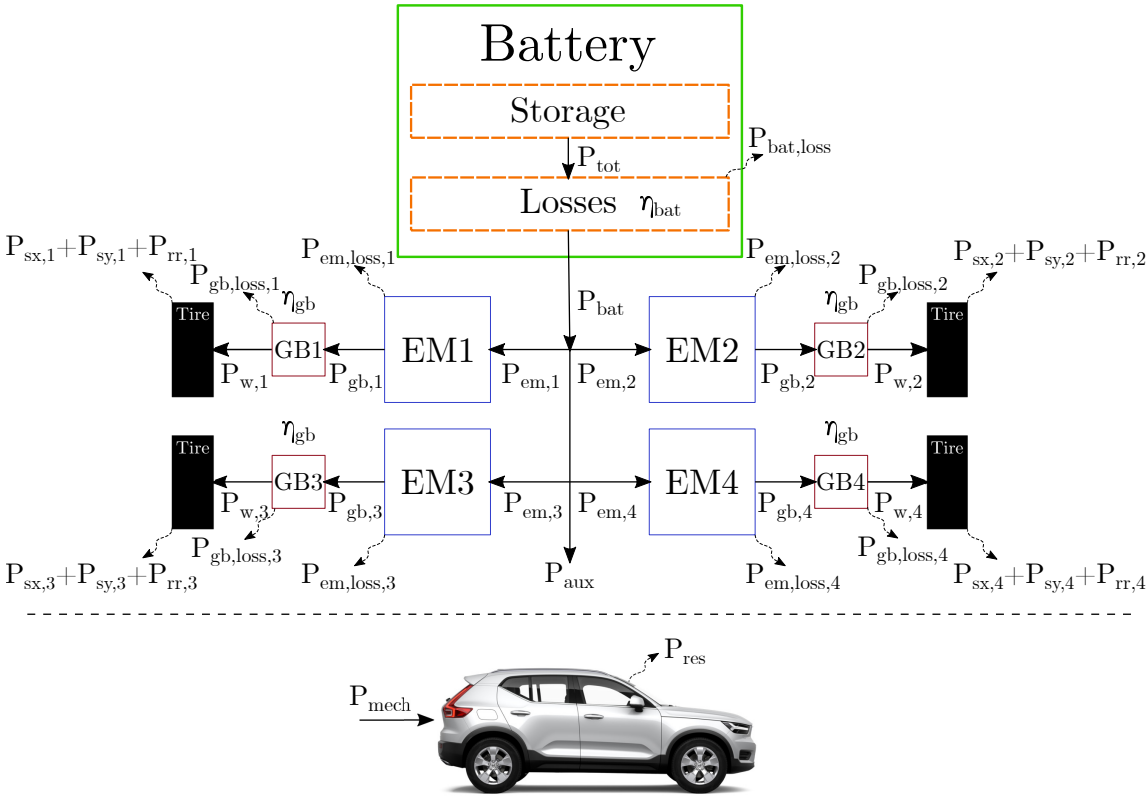

Figure 3.2: *Power flow.*

where η_{bat} is the round-trip efficiency of the battery and P_{bat} is the power going out from, or into, the battery. The round-trip efficiency is the ratio of the energy taken out of the system to the energy put into the system, i.e. $P_{bat,out}/P_{bat,in}$.

$$P_{bat} = \sum_{i=1}^{4} P_{em,i} + P_{aux} \tag{3.3}$$

where $P_{em,i}$ is the input power to electric motor $i \in \{1, ...4\}$ and P_{aux} is power to auxiliary systems such as air conditioning, music player etc. This is neglected in present thesis, and thus $P_{aux} = 0$. The power going into the electric motors is calculated through:

$$P_{em,i} = P_{gb,i} + P_{em,loss,i}, \quad i \in \{1...4\} \tag{3.4}$$

Where $P_{gb,i}$ is the input power to gear box, and $P_{em,loss,i}$ is the power loss of electric motor and inverter pair $i \in \{1, ..., 4\}$. The power going into the gear box is found by:

$$P_{gb,i} = \begin{cases} \frac{P_{w,i}}{\eta_{gb}}, & \text{if } P_{w,i} \leq 0 \\ \eta_{gb} P_{w,i}, & \text{if } P_{w,i} > 0 \end{cases} \tag{3.5}$$

where $P_{w,i}$ is the power input to the wheels and η_{gb} is the efficiency of the transmission. In Paper I the transmission efficiency is fixed (as presented in table 3.1) while it is derived from measurements in Paper II. The total power input to the wheels is expressed as:

$$\sum_{i=1}^{4} P_{w,i} = \sum_{i=1}^{4} \left(P_{sx,i} + P_{sy,i} + P_{rr,i} \right) + P_{mech} + P_{res} \tag{3.6}$$

where P_{mech} is the total power required to move the vehicle, $P_{sx,i}$ is the power lost to longitudinal slip, $P_{sy,i}$ is the power lost to lateral slip, $P_{rr,i}$ is the power lost to rolling resistance for $i \in \{1, ..., 4\}$, and P_{res} is the power lost due to resistances such as aerodynamic drag, friction in bearings etc.

3.1.2 Driving scenario

The driving pattern is a combination of the driver model and the chosen drive cycle. The driver model in CarMaker follows a predefined path and velocity profile which is given in the road definition of the drive cycle. The driver model represents a moderate driver and is limited within the following longitudinal and lateral acceleration ranges:

$$a_x \in [-4m/s^2, 3m/s^2]$$
$$a_y \in [-4m/s^2, 4m/s^2]$$

Gothenburg City Cycle (GCC) is a 66km long city cycle representing everyday driving in the vicinity of Gothenburg. It includes driving in residential areas with stop signs and speed breakers as well as highway segments. It was originally developed for analysis of everyday load on transmission and drive shafts, making it suitable for the purposes of this work. The velocity profile of GCC can be seen in figure 3.3(a).

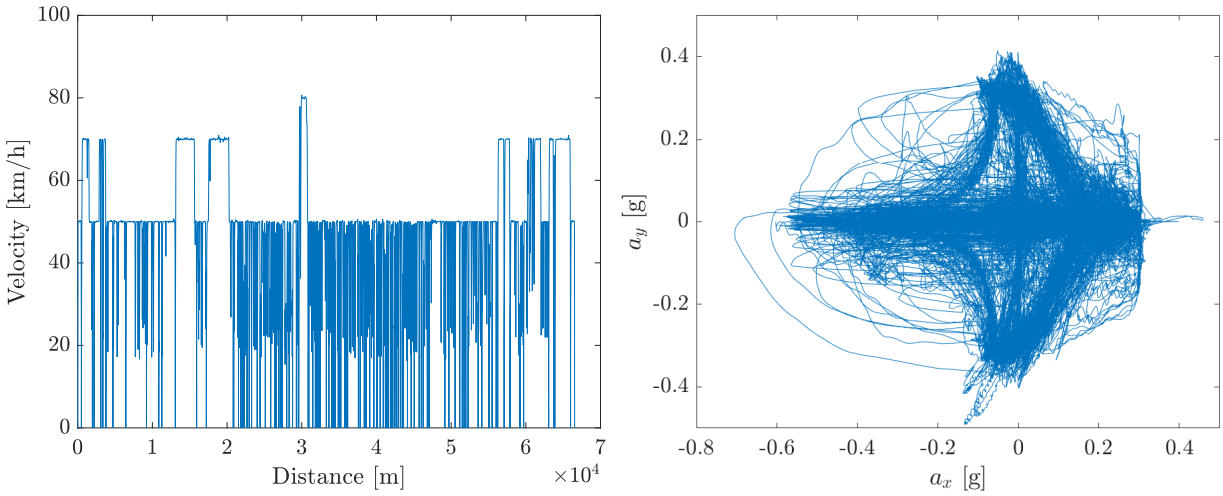

(a) *Velocity profile GCC.* **(b)** *gg-diagram GCC*

Figure 3.3: *Driving pattern of Gothenburg City Cycle (GCC)*

The gg-diagram of the driver model in combination with the drive cycle is shown in figure 3.3(b). As can be seen, the driver is constrained to the acceleration levels defined previously except for some outlying events during braking. The diagram also depicts that there are not many occurrences with a combination of higher longitudinal and lateral acceleration in the drive cycle, i.e. a change in speed during a curve is not common. Thus, the driving pattern represents a moderate driver in an everyday drive cycle.

3.2 Control Architecture

The control architecture is the framework in which vehicle control algorithms communicate with each other, with sensors and with actuators. The control architecture is a part of the larger function architecture, which includes actuators, sensors and possible mechanical control elements, such as hydro-mechanical brake system and steering column. Historically, vehicles were hardwired in the sense that every actuator had a specific purpose with its own request flow, often combined mechanical and algorithm based request flow. As the number of functions monitoring vehicle motion that use the same actuators increases, the resulting control architecture becomes increasingly

complex.

3.2.1 A good control architecture

One of the strengths of control allocation is that the actuator selection task is separated from the regulation task in the control design [4]. This implies the use of a hierarchical control architecture in the sense that the regulation of vehicle states is done prior and separate from the actuator *coordination*. Coordination in present thesis means the process of deciding which actuator receives input requests. This type of control architecture is beneficial not only in control allocation but in the *arbitration* of actuator requests from several different vehicle control algorithms. Arbitration here means how different requests from the mentioned *several* control algorithms are prioritized and balanced to *one* request. As vehicles become increasingly electronically controlled, there are several control algorithms that use the same actuators. For example, the electronic stability control function (ESC) uses brakes as a mean of fulfilling its control algorithm's actuator request. If the driver applies brake at the same time, the brake request from the driver and ESC is arbitrated in the brake control management (BCM), i.e. at actuator level. There may be additional control algorithms using brakes, e.g. adaptive cruise control, that also send brake requests to BCM which has to be taken into consideration when arbitrating the final actuator request. The development of the arbitration algorithm is done by the brake manufacturer delivering the BCM control unit, which makes migration of the algorithm or of actuator less easy. Thus, to allow for further development of old and new vehicle control algorithms and to facilitate the implementation in the existing software framework in vehicles, a hierarchical control architecture is necessary.

The authors in [15] have made an extensive review on integrated vehicle dynamics control architectures. It was shown that the main difference is the position of the coordination layer in the architecture. Their definition of coordination coincides with the definition of arbitration in present thesis. Hence, for consistency and readability here, coordination is substituted with arbitration. Two different approaches are defined to handle the combination of actuators in architecture; *downstream arbitration* and *upstream arbitration*. In downstream arbitration, driver input enters different vehicle subsystems (e.g. ESC, torque vectoring (TV), electronic power assist (EPAS), etc.) and the interaction between them is studied and arbitrated after the different

vehicle subsystems has generated their commands. It is presently dominant in vehicles as it is less complex, i.e. rule-based, where rules have successively been developed and added to the arbitration algorithm as vehicle subsystems have been developed and implemented. In upstream arbitration, the driver input enters the arbitration layer and the commands are arbitrated prior to the subsystems in a way to avoid conflicts further downstream. Upstream arbitration is more suitable for over-actuated vehicles with multiple actuators as well as for autonomous vehicles with multiple customer motion requests. The authors recommend a multi-layer architecture with control allocation to fulfill a reusable and generic architecture.

In [16], a three-layer hierarchical control architecture is proposed including three functional layers; the top layer includes functional elements such as the driver interpreter, vehicle motion control etc. that coordinates lower level functions in the mid-layer. Such lower level functions are the driver interface, the chassis which includes all the vehicle motion actuators etc. The lower layer is the actuator and sensor layer. In figure 3.1, the driver interpreter is represented by the reference generator in the top layer, the chassis is represented by the control allocator in the mid-layer and the actuator control represents the actuator layer. This three-layer approach is also used in [17, 18].

Thus, a hierarchical control architecture is an appropriate architecture for the problem considered in this thesis, i.e. a problem involving over-actuated vehicles.

3.3 Reference generator

The driver controls the vehicle's planar motion through the accelerator pedal, brake pedal and steering wheel angle. The reference generator uses these signals as inputs, $\mathbf{d}_{\text{req}}$, to interpret the driver's desired vehicle motion and generates longitudinal force, lateral force and yaw torque requests.

$$\mathbf{d}_{\text{req}} = [AccPdlPos, BrkPdlPos, \delta_{swa}] \tag{3.7}$$

where AccPdlPos and BrkPdlPos is the position of the accelerator and brake pedal, and δ_{swa} is the steering wheel angle.

The reference generator control of the vehicle is feed-forward, i.e. there is no feedback of vehicle states to the reference generator where the reference generator tries to minimize an error between desired and actual vehicle state. Feed-forward control has several advantages, for example a fast response time and relative insensitivity to signal disturbances from sensors. Perfect signal quality is seldom the case in vehicle motion control and estimation of states can be complicated. Hence, electronic feed-forward control is more robust and the feedback is left to the driver which closes the control loop by increasing the pedal positions or steering wheel angle if desired motion is not met.

3.3.1 Longitudinal motion

The driver controls the longitudinal motion through the accelerator and brake pedal. Hence, the request for longitudinal force is generated by using the positions of the pedals.

$$F_{x,req} = \gamma_1 AccPdlPos - \gamma_2 BrkPdlPos \tag{3.8}$$

where γ_1 and γ_2 are constant gains.

3.3.2 Lateral motion

The lateral motion reference is generated by a front wheel steered one-track dynamic model with constant longitudinal velocity and assuming no longitudinal forces. The model can be seen in figure 3.4. This type of model is a common choice for a reference model since its behavior is easy to predict by the driver due to its linear qualities.

The equations of planar motion are defined accordingly,

$$m(\dot{v}_y + v_x\omega_z) = F_{yf} + F_{yr} \tag{3.9}$$

$$I_{zz}\dot{\omega}_z = F_{yf}l_f - F_{yr}l_r \tag{3.10}$$

where m is the mass of the vehicle, v_y is the lateral velocity, v_x is the longitudinal velocity, ω_z is the yaw rate, F_{yf} and F_{yr} the front and rear lateral force.

$$F_{yf} = f_{yf}\cos\delta_f \tag{3.11}$$

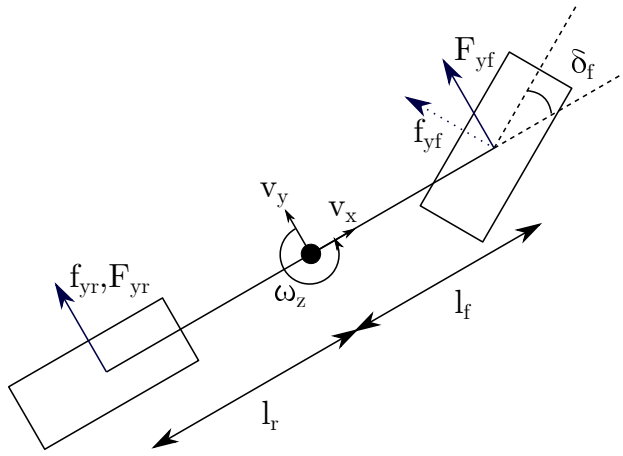

Figure 3.4: *One-track vehicle model.*

$$F_{yr} = f_{yr} \tag{3.12}$$

$$f_{yf} = -2C_{yf}\left(\arctan\left(\frac{v_y + l_f\omega_z}{v_x}\right) - \delta_f\right) \tag{3.13}$$

$$f_{yr} = -2C_{yr}\arctan\left(\frac{v_y - l_r\omega_z}{v_x}\right) \tag{3.14}$$

Where the tire cornering stiffness C_{yf} are C_{yr} are multiplied by 2 to represent axle cornering stiffness. The cornering stiffness used here are estimated from the vehicle model. Inserting (3.11) - (3.14) into (3.9) and (3.10) in combination with the small angle approximation ($\cos\delta = 1$), the following state-space model is defined.

$$\begin{bmatrix}\dot{v}_y \\ \dot{\omega}_z\end{bmatrix} = \begin{bmatrix}-\left(\frac{C_{yf}+C_{yr}}{mv_x}\right) & \frac{C_{yr}l_r - C_{yf}l_f}{mv_x} - v_x \\ \frac{C_{yr}l_r - C_{yf}l_f}{I_{zz}v_x} & -\left(\frac{C_{yf}l_f^2 + C_{yr}l_r^2}{I_{zz}v_x}\right)\end{bmatrix}\begin{bmatrix}v_y \\ \omega_z\end{bmatrix} + \begin{bmatrix}\frac{C_{yf}}{m} \\ \frac{C_{yf}}{I_z}\end{bmatrix}\delta_f \tag{3.15}$$

The front wheel angle (δ_f) is the input to the state-space model (3.15) which is found by dividing the steering wheel angle with a steering ratio.

$$\delta_f = \frac{\delta_{swa}}{r_{steer}} \tag{3.16}$$

The lateral force and yaw torque request can then be generated using the derivatives of lateral velocity and yaw rate from the state-space model.

$$F_{y,req} = m\left(\dot{v}_y + v_x\omega_z\right) \tag{3.17}$$

$$M_{z,req} = I_{zz}\dot{\omega}_z \tag{3.18}$$

3.4 Control Allocator

As stated previously in 2.3, two approaches to optimization based control allocation are developed and presented here. The first approach uses online optimization in the form of a quadratic program to minimize power losses online, i.e. at every simulation time step. The second approach uses a brute force offline optimization that generates an electric drive mode map used online in simulation.

Both approaches use the same objective function which is defined as a sum of the power losses in the electric motor, inverter, and tires. In Paper II the transmission losses and lateral slip losses are also included in the objective function. The expression for total power losses are

$$P_{loss} = P_{el} + P_{rr} + P_{s_x} + (P_{gb} + P_{sy}) \tag{3.19}$$

where P_{el} is the electrical power losses of the motors and inverters, P_{rr} is the power losses due to rolling resistance, and P_{s_x} is the power losses due to longitudinal tire slip, P_{sy} is the power loss due to lateral slip and P_{gb} are the transmission losses.

The optimization problem is defined as

$$\mathbf{u}_{\text{opt}} = \arg\left(\min_{\mathbf{u}} P_{loss}(\mathbf{u})\right) \tag{3.20}$$

$$\text{such that } \mathbf{Bu} = \mathbf{v}_{\text{req}} \tag{3.21}$$

The virtual control input, $\mathbf{v}_{\text{req}}$, contains the global vehicle force and torque requests and is defined below.

$$\mathbf{v}_{\text{req}} = \begin{bmatrix} F_{x,req} \\ F_{y,req} \\ M_{z,req} \end{bmatrix} \tag{3.22}$$

where $F_{x,req}$ is the longitudinal force request, $F_{y,req}$ is the lateral force request and $M_{z,req}$ is the yaw torque request.

The output from the control allocator, i.e. the control variables $\mathbf{u}_{\text{opt}}$ (the requests to the actuators), is given by (3.23).

$$\mathbf{u}_{\text{opt}} = \begin{bmatrix} \tau_{m,1} \\ \tau_{m,2} \\ \tau_{m,3} \\ \tau_{m,4} \\ \delta_f \end{bmatrix} \tag{3.23}$$

where $\tau_{m,i}$ is the motor request $i \in \{1, ..., 4\}$ and δ_f is the front wheel angle request.

3.4.1 Power Loss, P_{loss}

The power losses to be minimized in the cost function origin from the electric powertrain and the tires. In Paper I, the power losses in the electric powertrain (excluding transmission), the rolling resistance and longitudinal slip power losses are included. In Paper II, the cost function is expanded with the transmission power losses and lateral slip power losses. The power losses will be described briefly here and more detailed information about how the losses are reformulated to fit into the control allocation problem is found in the appended papers.

Battery power loss

In this thesis, it is assumed that all four electric motors draw their power from the same battery. The battery power loss does not affect the optimal momentaneous torque distribution since it is a result of the total power drawn by the motors, but it affects the total energy consumption. Hence, it is not included in the power loss cost function but it is included in the vehicle model.

Electric power loss

The losses in the electric powertrain, i.e. the electric motor and inverter, origin from e.g. heating of electric components (resistors, capacitors, etc.), friction and magnetic losses in the windings and core of the motor. In this thesis, the power losses are experimentally measured in a test-bench, see figure 3.5, resulting in a two-dimensional matrix dependent on rotational speed and applied torque. Since the losses are measured, they include the combined effect of the power loss processes present. In Paper I, the electric power loss used in the offline optimization, described in section 3.4.4, is found through linear interpolation. In the control allocator using online optimization, the power loss data was fitted with quadratic polynomials which are used in the cost function of the quadratic program described in section 3.4.3 The data is fitted with a separate polynomial for each rotational speed the measurement was performed at, resulting in 12 polynomials. Furthermore, separate curve fits are used for positive and negative torques. The control allocator compares the current rotational speed of the motor with the discrete measurement speeds and selects the polynomial associated with the speed that is closest, for positive or negative torque dependent on the longitudinal force request.

Rolling resistance power loss

Rolling resistance occurs due to hysteresis in the tire, i.e. when the deformation energy is larger than the recovery energy. Rubber elements in a rotating tire deflect upon coming into contact with the ground which due to its flexibility builds up a storage of potential energy. As the rubber element travels through the contact patch and leaves it, it will spring back out and regain its shape. However, due to damping in the rubber some of the potential energy is converted to heat, thereby contributing to the total power loss. Rolling resistance is dependent on tire load, tire construction, temperature and tire pressure as well as on applied torque. Rolling resistance is always present in a rolling tire. The rolling resistance power loss is expressed as:

$$P_{rr} = \sum_{i=1}^{4} -M_{yi}\omega_{wi} \tag{3.24}$$

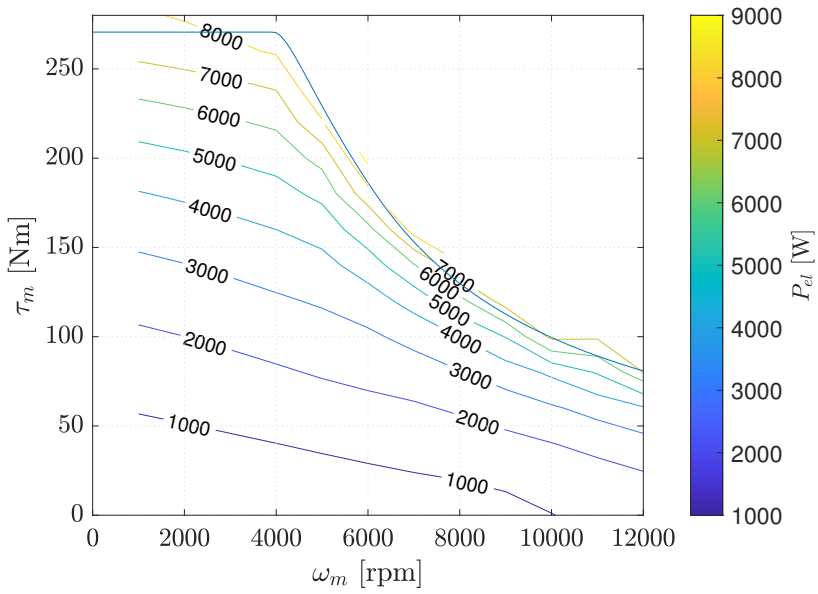

Figure 3.5: *Test bench measured power loss data for a typical single electric motor and inverter pair.*

where M_{yi} is the rolling resistance moment defined as equation (3.25) and ω_{wi} is the rotational speed of of the wheel.

$$M_{yi} = -F_{zi} r_0 \left\{ q_{sy1} + q_{sy2} \frac{F_{xi}}{F_{z0}} + q_{sy3} \left| \frac{v_{xi}}{v_{ref}} \right| + q_{sy4} \left(\frac{v_{xi}}{v_{ref}} \right)^4 \right\} \tag{3.25}$$

where F_{zi} is the vertical load of the tire, v_{xi} the longitudinal velocity of the wheel center and the remaining parameters r_0, $q_{sy1} - q_{sy4}$, F_{z0} and v_{ref} are acquired during experimental tire measurement. The values of these parameters are found in Paper I.

Tire slip power loss

In order for longitudinal and lateral forces to be generated, deflection of the rubber elements in the tire is needed. For the longitudinal direction, this deflection is caused by a difference in tire tangential speed and longitudinal speed of the wheel center relative to the ground, i.e. tire slip, of the contact

patch. The surface of the rubber elements sticking to the ground in the contact patch will follow the global vehicle longitudinal velocity while the upper part of the rubber element will follow the rotational velocity of the tire. In case of positive torque (propulsion), the tire will rotate faster than the longitudinal velocity, and the opposite is true when a negative torque is applied (braking). The rubber element acts like a spring, and as it is deformed shear stress develops which generates a force. Tire slip is necessary for forces to develop, but it also leads to power loss referred to as longitudinal slip power loss. Depending on normal load and tire stiffness, less deflection (i.e. less tire slip) of the rubber elements is needed to produce the same longitudinal force. Hence, the amount of longitudinal slip power loss can be affected by active torque distribution. The longitudinal slip power loss is expressed as:

$$P_{sx} = \sum_{i=1}^{4} f_{xi}(\omega_{wi} r_e - v_{xi}) \tag{3.26}$$

where r_e is the effective rolling radius.

In the lateral direction the difference between the steering angle of the wheel (where the wheel is pointing) and the direction of travel of the wheel (where the wheel is heading), i.e. the slip angle, causes the deflection of the rubber elements. Steering of the wheels is necessary to generate lateral forces but will also contribute to a force working against the direction of motion of the vehicle resulting in a power loss referred to as lateral slip power loss, also known as *cornering resistance* [19]. Similar to the longitudinal case, normal load and tire stiffness will lead to less deflection of the rubber elements needed to produce equal lateral force. Thus, the steering angles of the wheels can be distributed in such a way to minimize lateral slip power loss. It is expressed accordingly:

$$P_{sy} = \sum_{i=1}^{4} f_{yi} v_{ywi} \tag{3.27}$$

where v_{ywi} is the lateral velocity in the wheel coordinate system.

Transmission power loss

The transmission power losses origin from friction in the gears. In Paper I, the transmission losses are represented by a fixed efficiency, 97% as in [20], and are not included in the cost function. In Paper II they are, similar to the electric power losses, experimentally measured in a test-bench. The transmission losses are fitted with a separate quadratic polynomial for each rotational speed the measurement was performed at, resulting in 7 polynomials. The curve fit is done separately for positive and negative torque. The control allocation algorithm then compares current rotational speed of the motor and selects the polynomial associated with the speed that is closest. This polynomial is used in the cost function of the quadratic program described in section 3.4.3.

3.4.2 Control Effectiveness Matrix, B

The control allocator will find the most energy efficient solution under the condition that the requests defined in the virtual control input $\mathbf{v}_{\text{req}}$ are fulfilled. Thus, a relationship between the control variables and vehicle motion needs to be established. This relationship is in the form of a control effectiveness matrix, referred to as the *B-matrix*. The relationship between the control variables and the virtual control needs to be linear according to (3.21). It is based on a two-track vehicle model presented in figure 3.6 and the planar equations of motion are derived below.

$$m\left(\dot{v}_x - v_y\omega_z\right) = F_{x1} + F_{x2} + F_{x3} + F_{x4} - F_{res} \tag{3.28}$$

$$m\left(\dot{v}_y + v_x\omega_z\right) = F_{y1} + F_{y2} + F_{y3} + F_{y4} \tag{3.29}$$

$$I_{zz}\dot{\omega}_z = \frac{w}{2}\left(-F_{x1} + F_{x2} - F_{x3} + F_{x4}\right) + l_f\left(F_{y1} + F_{y2}\right) - l_r\left(F_{y3} + F_{y4}\right) \tag{3.30}$$

where F_{xi} the longitudinal force of wheel corner $i \in \{1, ..., 4\}$ in vehicle coordinate system, F_{res} the driving resistance including e.g. aerodynamic drag and F_{yi} is the lateral force in vehicle coordinate system.

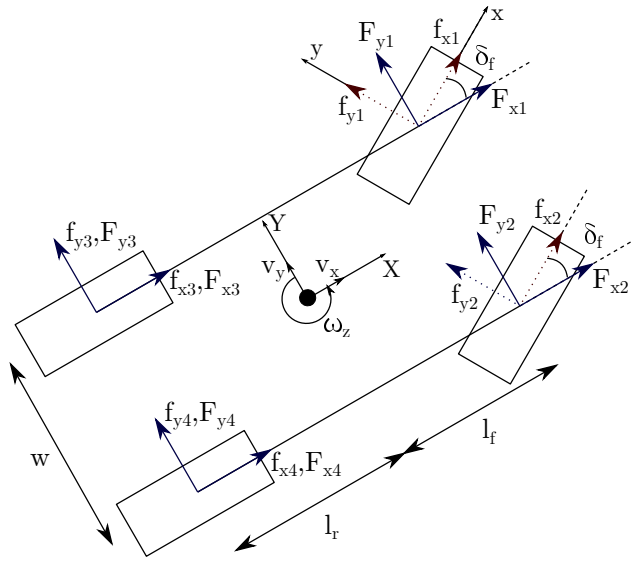

Figure 3.6: *Two-track vehicle model.*

The driver will decide the total required driving force including desired acceleration and compensation for driving resistance, hence equation (3.28) can be rewritten accordingly.

$$F_{x,req} = F_{x1} + F_{x2} + F_{x3} + F_{x4} \tag{3.31}$$

where $F_{x,req}$ is the virtual control input for longitudinal motion generated by the driver.

Similar to the longitudinal virtual control input, the lateral force and yaw torque request are generated by the driver through desired lateral and yaw acceleration. Thus, (3.29) and (3.30) are rewritten accordingly.

$$F_{y,req} = F_{y1} + F_{y2} + F_{y3} + F_{y4} \tag{3.32}$$

$$M_{z,req} = \frac{w}{2}\left(-F_{x1} + F_{x2} - F_{x3} + F_{x4}\right) + l_f\left(F_{y1} + F_{y2}\right) - l_r\left(F_{y3} + F_{y4}\right) \tag{3.33}$$

The longitudinal and lateral forces can be expressed in terms of wheel forces according to:

$$F_{xi} = f_{xi}\cos(\delta_i) - f_{yi}\sin(\delta_i) \tag{3.34}$$

$$F_{yi} = f_{xi}\sin(\delta_i) + f_{yi}\cos(\delta_i) \tag{3.35}$$

where f_{xi} and f_{yi} are the longitudinal and lateral tire forces in the wheel coordinate system as visualized in figure 3.6. The wheel forces can in turn be expressed as functions of motor torque and wheel angle according to:

$$f_{xi} = \frac{\tau_{wi}}{r_l} = \frac{\tau_{mi} n}{r_l} \qquad f_{yi} = -C_{yi}\alpha_i \tag{3.36}$$

$$\alpha_i = \beta_i - \delta_i \qquad \beta_i = \arctan\left(\frac{v_{yi}}{v_{xi}}\right) \tag{3.37}$$

where τ_{wi} is the wheel torque, τ_{mi} is the electric motor torque, n is the transmission ratio, C_{yi} the cornering stiffness, α_i the slip angle, β_i is the tire side slip angle, v_{yi} the lateral velocity and v_{xi} the longitudinal velocity of wheel corner $i \in \{1, ..., 4\}$. The longitudinal and lateral velocities for respective wheel corner are defined below.

$$v_{y1} = v_{y2} = v_y + l_f\omega_z \qquad v_{y3} = v_{y4} = v_y - l_r\omega_z \tag{3.38}$$

$$v_{x1} = v_{x3} = v_x - \frac{w}{2}\omega_z \qquad v_{x2} = v_{x4} = v_x + \frac{w}{2}\omega_z \tag{3.39}$$

Linearizing (3.34) and (3.35) around $\delta_i = 0$ (i.e. assuming small angles) generates the following expressions for wheel corner forces.

$$F_{xi} = f_{xi} - f_{yi}\delta_i \qquad F_{yi} = f_{xi}\delta_i + f_{yi} \tag{3.40}$$

By using the small angle approximation ($\cos\delta_i = 1$, $\sin\delta_i = \delta_i$, $\delta_i^2 = 0$, $\delta_i\beta_i = 0$) and (3.36), (3.37), the wheel corner forces (3.40) can be reformulated as expressions of motor torque and wheel angles.

$$F_{xi} = \frac{\tau_{mi} n}{r_l} \tag{3.41}$$

$$F_{yi} = \frac{\tau_{mi} n}{r_l}\delta_i - C_{yi}\beta_i + C_{yi}\delta_i \tag{3.42}$$

The expression for lateral force (3.42) includes a non-linear element between the control variables τ_m and δ. Since the control variables cannot be

coupled this element is neglected and removed from the expression resulting in (3.43).

$$F_{yi} = -C_{yi}\beta_i + C_{yi}\delta_i \tag{3.43}$$

Furthermore, the first term of (3.43) is not dependent on δ_i and can be seen as constant since it is independent of the control variables. All similar terms are gathered in a vector $\mathbf{c}$ which is subtracted from the virtual control input $\mathbf{v}_{\text{req}}$. With $\delta_1 = \delta_2 = \delta_f$ and $\delta_3 = \delta_4 = 0$ and assuming the same cornering stiffness left and right, the final B-matrix is defined according to (3.44).

$$\mathbf{B} = \begin{bmatrix} \frac{n}{r_l} & \frac{n}{r_l} & \frac{n}{r_l} & \frac{n}{r_l} & 0 \\ 0 & 0 & 0 & 0 & 2C_{yf} \\ -\frac{wn}{2r_l} & \frac{wn}{2r_l} & -\frac{wn}{2r_l} & \frac{wn}{2r_l} & 2C_{yf}l_f \end{bmatrix} \tag{3.44}$$

$$\mathbf{c} = \begin{bmatrix} 0 \\ -C_{yf}\left(\beta_1 + \beta_2\right) - C_{yr}\left(\beta_3 + \beta_4\right) \\ -l_f C_{yf}\left(\beta_1 + \beta_2\right) + l_r C_{yr}\left(\beta_3 + \beta_4\right) \end{bmatrix} \tag{3.45}$$

$$\mathbf{B}\mathbf{u} = \mathbf{v}_{\text{req}} - \mathbf{c} \tag{3.46}$$

3.4.3 Online optimization: Quadratic Program

The quadratic program (QP) has been chosen as the method for online optimization due to its convex properties provided a convex set of constraints. This means that the solution will not be stuck in local minima, and can be obtained analytically if the saturation limits of the actuators are disregarded. The optimization problem in the form of the quadratic program is formulated according to equation (3.47).

$$\mathbf{u}_{\text{opt}} = \arg\left(\min_{\mathbf{u}}\left(\frac{1}{2}\mathbf{u}^T\mathbf{Q}\mathbf{u} + \mathbf{f}^T\mathbf{u}\right)\right) \tag{3.47}$$

$$\text{such that } \mathbf{B}\mathbf{u} = \mathbf{v}_{\text{req}},$$

By introducing Lagrangian multipliers, $\boldsymbol{\lambda}$, the original optimization problem (3.47) is relaxed according to:

$$\begin{bmatrix} \mathbf{u}_{\text{opt}} \\ \boldsymbol{\lambda} \end{bmatrix} = \arg\left(\min_{\mathbf{u},\boldsymbol{\lambda}}\left(\frac{1}{2}\mathbf{u}^T\mathbf{Q}\mathbf{u} + \mathbf{f}^T\mathbf{u} + \boldsymbol{\lambda}^T\left(\mathbf{B}\mathbf{u} - \mathbf{v}_{\text{req}}\right)\right)\right) \tag{3.48}$$

where $\boldsymbol{\lambda}$ is a diagonal, symmetric matrix with the same dimension as the number of elements in $\mathbf{v}_{\text{req}}$. The optimization problem is now unconstrained and can be solved analytically through:

$$\begin{bmatrix} \mathbf{u}_{\text{opt}} \\ \boldsymbol{\lambda} \end{bmatrix} = \begin{bmatrix} \mathbf{Q} & \mathbf{B}^T \\ \mathbf{B} & \mathbf{0} \end{bmatrix}^{-1} \begin{bmatrix} -\mathbf{f} \\ \mathbf{v}_{\text{req}} \end{bmatrix} \tag{3.49}$$

The power losses are expressed as quadratic functions of the control variables where the first coefficient of the polynomial is stored in Q and the second coefficient of the polynomial stored in f. The derivations of rolling resistance power loss and longitudinal slip power loss are found in Paper I, and the derivation for lateral slip power loss is found in Paper II. The quadratic curve fit of the electric power losses include a term that is not dependent on applied torque and represents the power losses at zero torque. In order to include a coupling in the control allocation algorithm, three QPs are formulated for FWD, RWD and AWD respectively. In FWD, the rear motors are removed from the optimization problem, and in RWD the front motors are removed. The total power losses from the three different QPs are estimated, and the control algorithm chooses the torque distribution solution providing the lowest power losses. The online optimization method is applied both in Paper I and II with lateral and yaw motion added in the latter.

3.4.4 Offline optimization: Brute force

The offline optimization is based on the exhaustive search method, a.k.a. the brute force method. It results in a lookup table that is implemented in simulation. A map of operation points based on a range of total torque and electric motor speed is generated. For each operation point, the total power loss for a number of torque distributions is investigated under the constraint that the total torque is fulfilled. The torque distribution providing the lowest total power loss will be saved as the optimal torque distribution for that

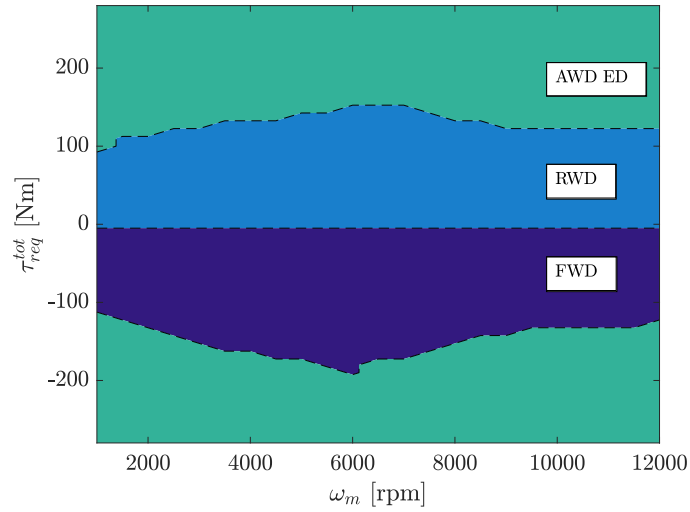

Figure 3.7: *Lookup table.*

operating point. The tire power loss expressions used here are the same as are used in QP, here with the static normal load. For the electric losses, as previously mentioned, linear interpolation is used between the data points in the experimental data. Thus the approximation of electric power loss is more accurate than in QP. It was found that the torque distributions were mainly divided into three modes; front wheel drive (FWD), all wheel drive with equal torque on each motor (AWD ED) and rear wheel drive (RWD), see figure 3.7. To simplify the lookup table, the torque distributions were limited to one of these three modes. A more detailed description of how the lookup table is generated and how the different losses affect the torque distribution can be found in Paper I. Worth noting is that this lookup table is specific for the transmission ratios used during its generation. With different transmission ratios front and rear, the distribution modes and mode switch limit may be different.

The lookup table is seen in figure 3.7. At low propulsion torque the RWD mode is the most efficient mode. The reason the rear axle is selected for propulsion torques is due to the rolling resistance moment being smaller at the axle with low normal load. The rolling resistance moment increases proportionally with applied torque resulting in less rolling resistance power loss

if the torque is applied to the axle with lower normal load. By moving the center of gravity towards the rear, hence making the normal load at the rear larger than the front, the optimization will favor the front axle during propulsion. The opposite is true for brake torque; at low brake torque the FWD mode is most efficient. Since the rolling resistance moment with applied torque, and is higher at the front axle, less applied brake torque is needed in order to slow down the vehicle. This also means less regeneration, but since the cost function only includes power losses, the power gained through regenerative braking is not taken into account during the optimization. At high propulsive and brake torques the AWD ED mode is most efficient.

In simulation, the input to the lookup table is total torque request and current velocity of the vehicle. The longitudinal force request by the driver is translated to a total torque request and the vehicle velocity is translated into motor rotational velocity. The output from the lookup table is the optimal torque distribution at that particular instant. The lookup table is applied in simulation in Paper I.

3.4.5 Actuator saturation

In this work, the actuator constraints are left out of the optimization problems in order to keep the simplicity of unconstrained optimization. The electric motors are saturated both by the maximum available torque but also by the maximum available friction force dependent on normal load of the tires and tire-ground friction.

When only considering control of the longitudinal direction (Paper I), the motor torques are limited to not contribute to a yaw torque on the vehicle body. If the torque is saturated on one axle, the remaining torque required to reach the longitudinal force request is distributed to the other axle. For example, the control allocator provides an optimal solution ($\mathbf{u}_{\text{opt}}$) to the longitudinal force request ($F_{x,req}$ in $\mathbf{v}_{\text{req}}$), which includes the use of the front motors only. The solution is infeasible since $\tau_{m,1}$ and $\tau_{m,2}$ are saturated. The algorithm then takes the remaining part of the longitudinal force request, i.e. $F_{x,req} - \frac{n}{rl}(\tau_{m,1} + \tau_{m,2})$, and distributes it evenly to the rear motors $\tau_{m,3}$ and $\tau_{m,4}$. When controlling the complete planar motion (Paper II), i.e. longitudinal, lateral and yaw control, the same approach is used. If a motor on one side is saturated, the remaining motor torque request is distributed

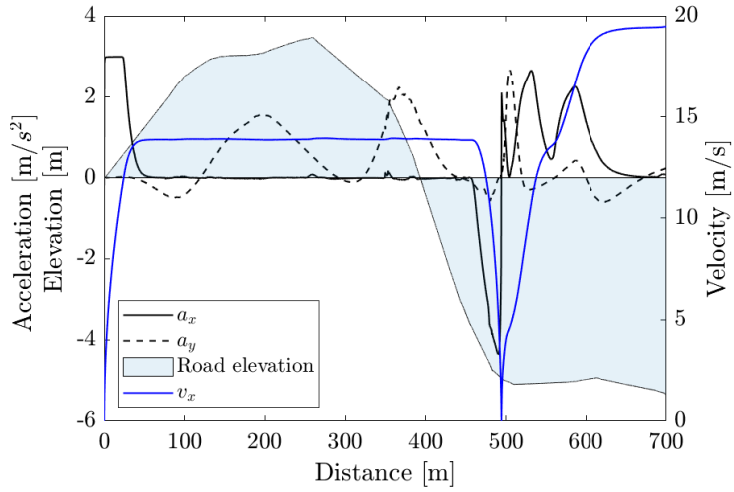

Figure 3.8: *Longitudinal and lateral acceleration, velocity and road elevation of a 700m long segment of GCC. The first 100m are used for presentation of wheel torques in Paper I.*

to the second motor on the same side. Hence, both the $M_{z,req}$ and $F_{x,req}$ will be fulfilled.

3.5 Validation of power loss models

One segment of GCC will be used while presenting the power losses and results in chapter 4. The longitudinal and lateral acceleration, velocity and road elevation as functions of traveled distance of the segment is shown in figure 3.8. The segment includes one acceleration event from standstill at 0-50m, negotiating curves at constant speed 50km/h at 50-470m, deceleration to standstill at 470-500m, a sharp low-speed turn 500-510m, and finally a second acceleration event at 510-600m.

The first step is to investigate if the power loss models approximated to quadratic functions of torque and wheel steering angle are sufficiently accurate. CarMaker provides power loss signals that are here assumed to be accurate enough and used for validation of the tire power loss models defined in 3.4.1. The estimated electric and transmission losses from the polynomials used in QP are compared to the losses from the test rig measurements.

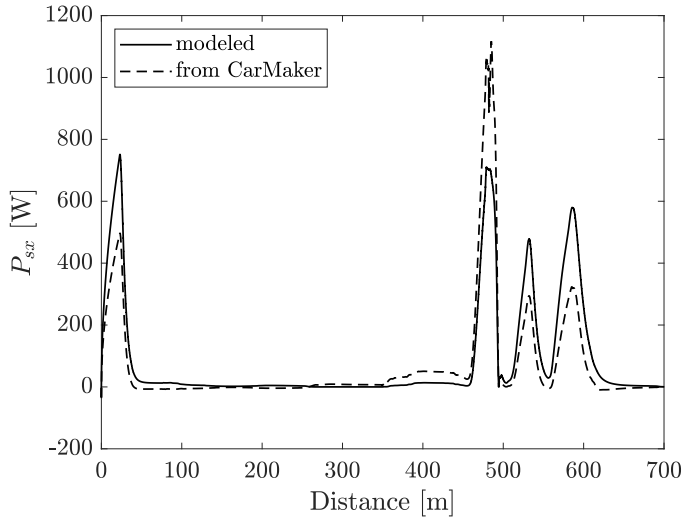

Figure 3.9: *Comparison of modeled longitudinal slip power loss and CarMaker signal. Propulsion: 0-450m and 500-700m, braking: 450-500m.*

A comparison between the modeled longitudinal slip power loss and the signal of longitudinal slip power loss from CarMaker is presented in figure 3.9. As can be seen, there is a deviation between the two signals. One reason for this deviation is the discrepancy between actual longitudinal force at the wheel and the estimated longitudinal force from the motor torque and wheel radius. The estimate do not account for resistive forces in the tires, resulting in greater values during propulsion to overcome the resistive forces (0-350m, 500-700m), and smaller during braking now aided by the resistive forces (350-500m). This can be seen in the figure as the model overestimates the losses during propulsion and underestimates during braking. Furthermore, the effective wheel radius and longitudinal tire stiffness are constant in the model, but will change during driving due to load transfer from longitudinal and lateral acceleration and road grade. The modeled longitudinal slip power loss does however follow the same pattern as the signal from CarMaker, and is quite small due to the moderate nature of the drive cycle. It is, therefore, a sufficient model for this work.

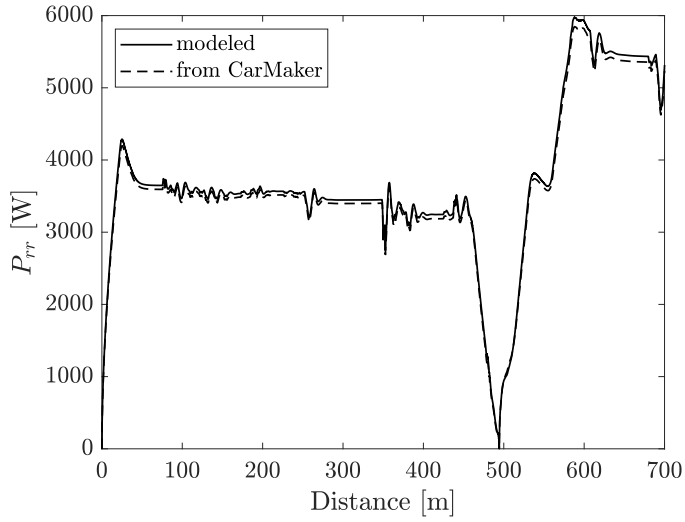

Figure 3.10: *Comparison of modeled rolling resistance power loss and CarMaker signal. Propulsion: 0-450m and 500-700m, braking: 450-500m.*

The model of rolling resistance power loss and the CarMaker signal match better, see figure 3.10. The deviations here can also be explained due to the estimate of longitudinal force, but since this component is not as prominent in the expression for rolling resistance power loss, it has less impact on the total rolling resistance power loss. In figure 3.11 a comparison between the modeled lateral slip power loss and CarMaker signal can be seen. These match very well.

The estimated electric losses compared to the measurement data can be seen in figure 3.12. The signals match well except for when the velocity is high and torque demand on the motors low (between 50-400m and after 600m). The deviation comes from the ill-fitting curve at higher velocities and low torque demand on the motors.

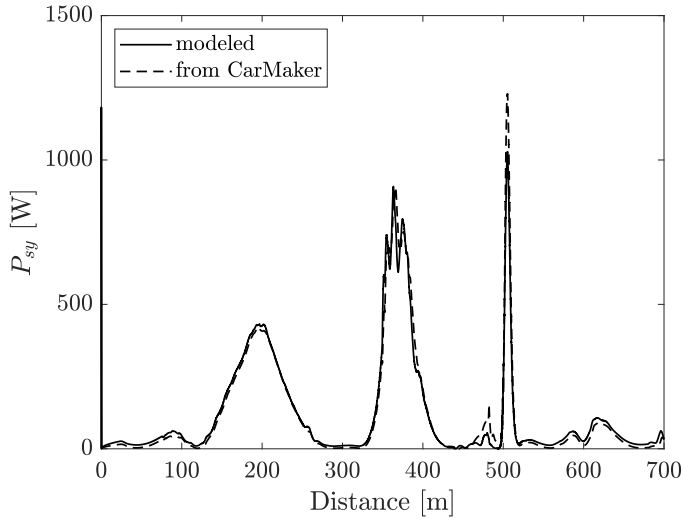

Figure 3.11: *Comparison of modeled lateral slip power loss and CarMaker signal. Propulsion: 0-450m and 500-700m, braking: 450-500m.*

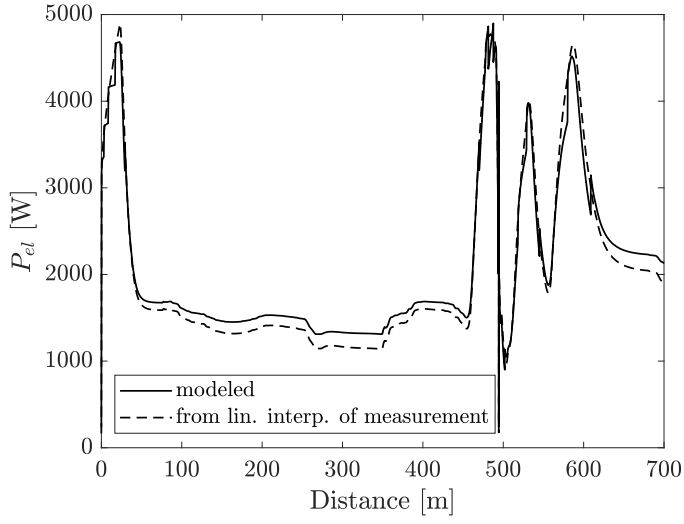

Figure 3.12: *Comparison of modeled electric power loss and measurement. Propulsion: 0-450m and 500-700m, braking: 450-500m.*

The estimated power losses from the transmission is compared to the measurement data in figure 3.13. Here, one can see where the control alloca-

tor changes the speed dependent polynomial, most clearly right before 500m and 600m. The gaps between the different speeds were quite large in the measurement data, resulting in these jumps. The transmission model in the vehicle uses linear interpolation between the data points, resulting in a more smooth curve.

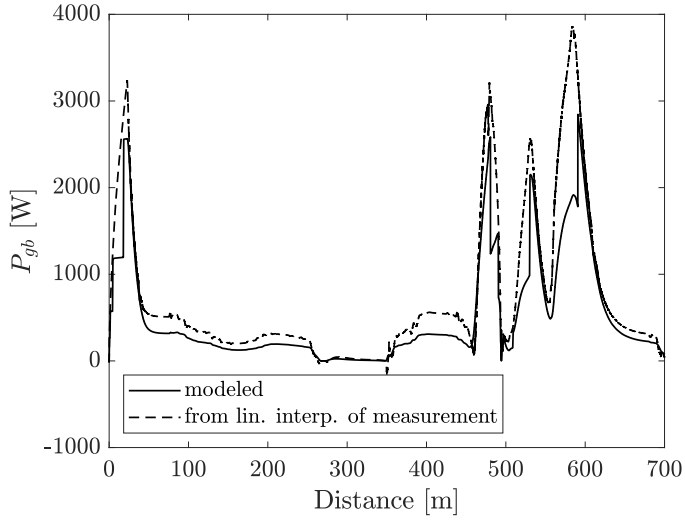

Figure 3.13: *Comparison of modeled transmission power loss and measurement. Propulsion: 0-450m and 500-700m, braking: 450-500m.*

Concludingly, it is clear from these figures that, in addition to the good match between the modeled power losses and the CarMaker signals or measurement data, the longitudinal and lateral slip losses are small relative to the electric and rolling resistance losses.

Chapter 4

Wheel force optimization

The aim is to control the vehicle's planar motion in the most energy efficient way. In order to do so, the first step is to verify that the control allocator provides the driver with desired motion in the form of planar forces and torque requests. In section 4.1, the requested planar forces and torque will be compared with the actual motion of the vehicle and possible discrepancies will be discussed. The longitudinal control is presented in 4.1.1 followed by the full planar motion including lateral and yaw control in 4.1.2. Then, the effect of different transmission ratios front and rear will be explored in 4.2 in terms of its effect on energy consumption. Lastly, the performance of the control allocation algorithms on energy efficiency will be presented in section 4.3.

4.1 Planar vehicle force and torque control

4.1.1 Longitudinal control (Paper I)

The longitudinal control of the vehicle is handled in Paper I. The control is a combination of feed-forward and feedback system where the driver is responsible for the feedback part. The reference used for comparison is even torque distribution on all four motors (ED). The same segment of GCC that was used for the power loss validations in section 3.5 is used here, seen in figure 3.8.

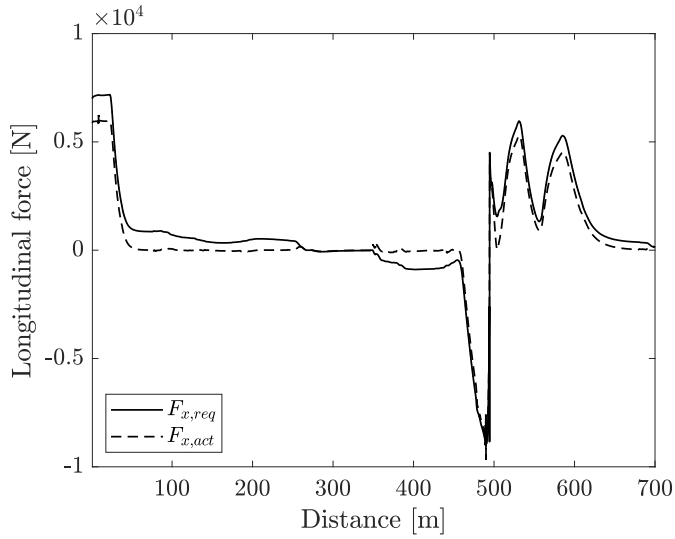

Figure 4.1: *Requested versus actual longitudinal force from CarMaker.*

A comparison between the requested and actual longitudinal force is presented in figure 4.1. During propulsion (0-450m and 510-700m), the requested longitudinal force $F_{x,req}$ is higher than the actual longitudinal force $F_{x,act}$, and the opposite during braking (350-500m). This is an effect of the control being feed-forward only. The controller (i.e. the reference generator) does not account for any resistive forces that occurs due to e.g. aerodynamic drag. During propulsion, these forces work against the desired direction of motion (increasing or keeping a constant speed) and hence the driver will increase the position on the accelerator pedal to reach it. In contrast, during a braking maneuver the resistive forces will work in favor of the desired direction of motion (slowing down), and hence the driver will not need to apply as much brake.

In figure 4.2, the motor torque distributed by the control allocator using the lookup table is compared to the control allocator using QP. As was seen in the lookup table, the control allocator distributes low propulsion torque to the rear motors (see figure 4.2(a), 50-450m and 600-700m), and when the demand reaches a certain torque limit it is changed to equal torque distribution (0-50m, 520-550m and 570-600m). With the control allocator using QP, see figure 4.2(b), the transition from two motors to four motors happens slightly

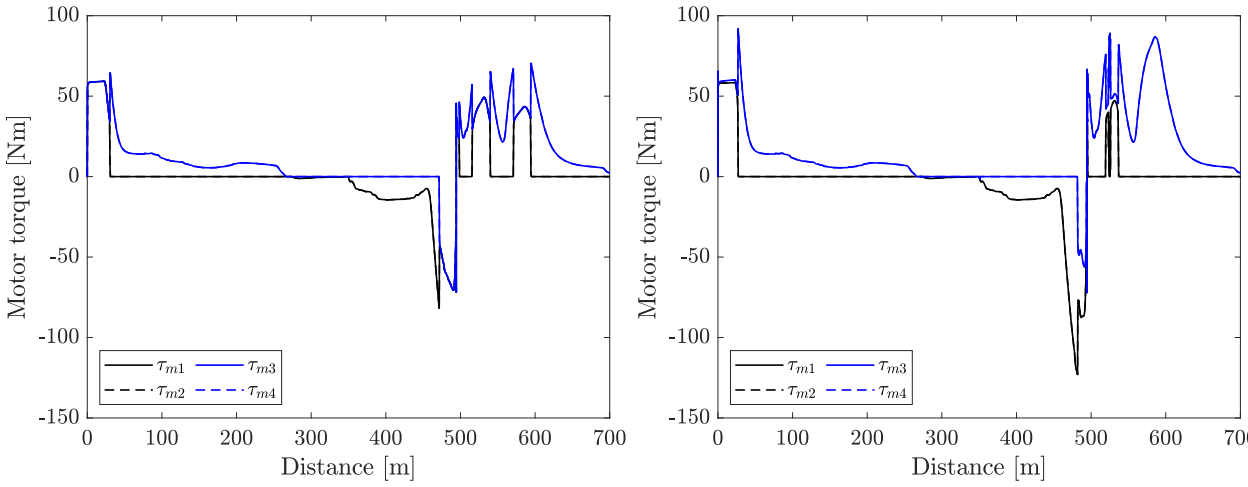

(a) *Lookup.* **(b)** *QP*

Figure 4.2: *Torque distribution resulting from the offline optimization and online optimization.*

earlier. This is due to the quadratic curve fit of the electric power losses. For the brake maneuver (350-500m), low brake torque demand is distributed to the front motors, and high brake torque demand is distributed evenly on all four motors, as was also depicted by the lookup table. Here, the control allocator using QP switches to four motors later than the control allocator using the lookup table. The two-motor torque distribution range is wider for the control allocator using QP compared to the one using the lookup table, hence it switches earlier from four to two motors during propulsion and from two to four motors later during braking.

4.1.2 Longitudinal, lateral and yaw control (Paper II)

By introducing lateral and yaw movement as controllable degrees of freedom, and wheel steering angles as control variables, the driver becomes mechanically disconnected from the control of the vehicle. The complete control of vehicle planar motion is now handled by the control allocator. The reference used here is once more equal torque distribution, and equal front steering angles right and left, translated from the driver SWA input through a steering ratio.

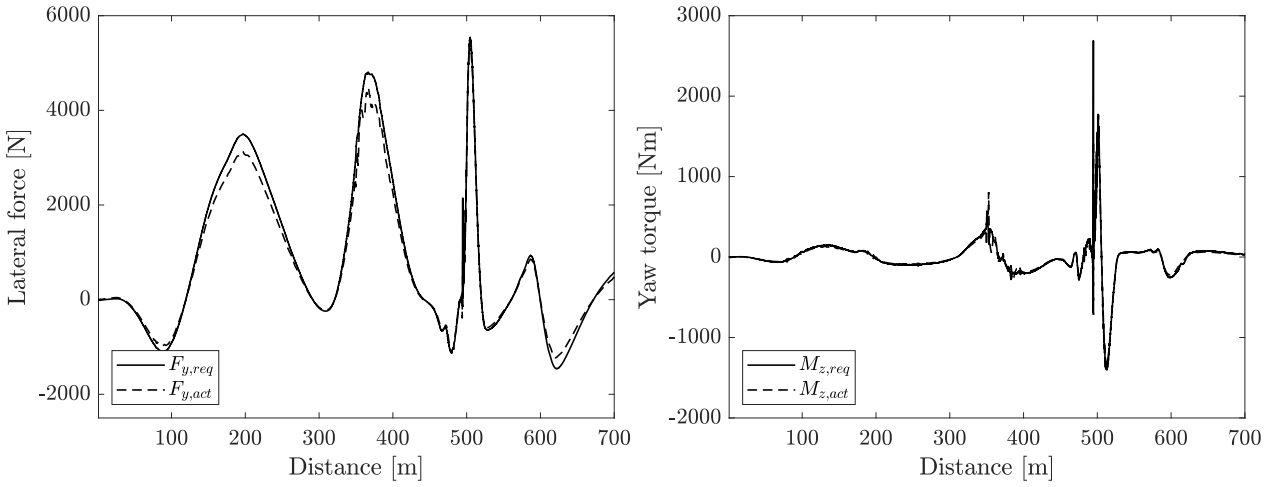

(a) *Lateral force.* **(b)** *Yaw torque.*

Figure 4.3: *Requested versus actual lateral force and yaw torque.*

The requested and actual lateral force and yaw torque from CarMaker is presented in figures 4.3(a) and 4.3(b) respectively. Once more, one can see that the requested force/torque is higher than the actual as a result of resistive forces in the system which are not accounted for in the feed-forward control. Apart from this discrepancy, one can conclude that the control allocator successfully fulfills the driver's request on vehicle motion.

In Paper II, it was discovered that there is an issue with the lateral force and yaw torque request for the purposes of power loss minimization. The vehicle model used in the reference generator is front wheel steered, and $F_{y,req}$ and $M_{z,req}$ generated are coupled by the front wheel steering angle. Only the front wheel steering angle can fulfill $F_{y,req}$ according to the B-matrix (equation (3.44), which will also fulfill the $M_{z,req}$ since the yaw torque request was generated with the same steering angle. Hence, the front wheel steering angle solution is already decided prior to the optimization in the control allocator, it is unique. Since the wheel angle fulfills both $F_{y,req}$ and $M_{z,req}$, the is no room for minimization of power losses through differential torque between left and right side of the vehicle. However, this does not mean that the control allocator can't provide solutions where $F_{y,req}$ and $M_{z,req}$ are decoupled.

In fact, if $M_{z,req}$ is increased by 20% while leaving $F_{y,req}$ intact, one can see that the control allocator will apply differential torque left and right to fulfill this increased yaw torque request.

By extending the control variables further with rear wheel steering angles, the potential for saving energy can be improved even more. In [21], it was shown that introducing rear wheel steering can improve energy efficiency by 8.4% as opposed to only using front wheel steering angles and equal wheel torque on all four wheels. Worth noting is that in this study a single lane change maneuver was used which is a very limited representation of everyday driving, and the path was optimized in order to reduce total power rather than basing the vehicle motion request on driver input. The potential of using rear wheel angles for the purpose of energy efficiency is, however, clear. Another important aspect of this is how the driver will experience the motion, i.e. if it will find the maneuver comfortable or not. Energy efficient driving does not necessarily imply a comfortable ride.

The introduction of rear steer angles in the control variable space requires a more complex optimization method. The linearity concerning steering angles in the B-matrix overlooks important non-linear relationships between longitudinal wheel force and steering angles. For example, the longitudinal force of a wheel corner in vehicle coordinates is a non-linear product of longitudinal wheel force in wheel coordinates and steering angle according to equation (3.34). This relationship tells us that increasing the angle of the wheel will require more longitudinal wheel force in order to produce the same longitudinal wheel corner force. By linearizing the B-matrix the control allocator will not see this effect. This might result in an increase in wheel angles to minimize lateral power losses, which in turn will lead to the driver applying more gas to reach desired longitudinal motion. Clearly, this is not energy efficient as the driver now requests higher total motor torque. The whole maneuver in itself is more expensive energy-wise. Hence, in order to incorporate rear steering angles in the control allocator the optimization method needs to allow non-linear relations between the control variables.

4.2 Changing transmission ratio (Paper II)

The study of transmission ratio was performed by designing a full factorial matrix with transmission ratios front and rear ranging from 6 to 14 in steps of 2, resulting in 25 transmission ratio combinations. Each combination was applied to the vehicle model, simulated in GCC and the energy consumed was recorded. The combination with the least amount of energy consumed was declared as the optimal one.

For equal wheel torque distribution, it was found that the optimal transmission ratio was 12 both in the front and in the rear. Performing the full factorial in combination with the control allocator using QP without the ability to decouple motors from the wheels resulted in the same optimal transmission ratio combination: 12 in the front and in the rear.

In contrast, the most optimal transmission ratio combination resulting from the full factorial in combination with QP **with** the ability decouple the motors from the wheels is different. Here, the optimal transmission ratio is 14 in the front and 10 in the rear. In figure 4.4(a), the torque distribution when the transmission ratio is 12 in the front and rear is shown, and in 4.4(b) when the transmission ratio is 14 in the front and 10 in the rear. It can be seen in 4.4(a) that during propulsion, the two rear motors are most optimal to use, and during braking the front motors should be used. With transmission ratio 14 in the front and 10 in the rear, however, the front motors are used during high torque demands as this requires lower motor torque compared to using the rear motors. As the velocity increases and the torque demand decreases (50-450m, 550-700m), the rear motors with lower transmission ratio are used.

By only considering the electric power losses, in acceleration maneuvers it is most energy efficient to use the motors with the highest transmission ratio as this requires the least amount of motor torque. During highway driving, i.e. higher velocities with low torque, it is beneficial to use the motors with lower transmission ratio, as these will rotate slower than the motors with higher transmission ratio, and decouple the other motors. Thus, only looking at the electric power losses, it shouldn't matter whether the front or rear motors have the lower or higher transmission ratio. However, when considering the tire losses the outcome is different. As mentioned previously, it was found that the optimal transmission ratio is 14 in the front and 10 in

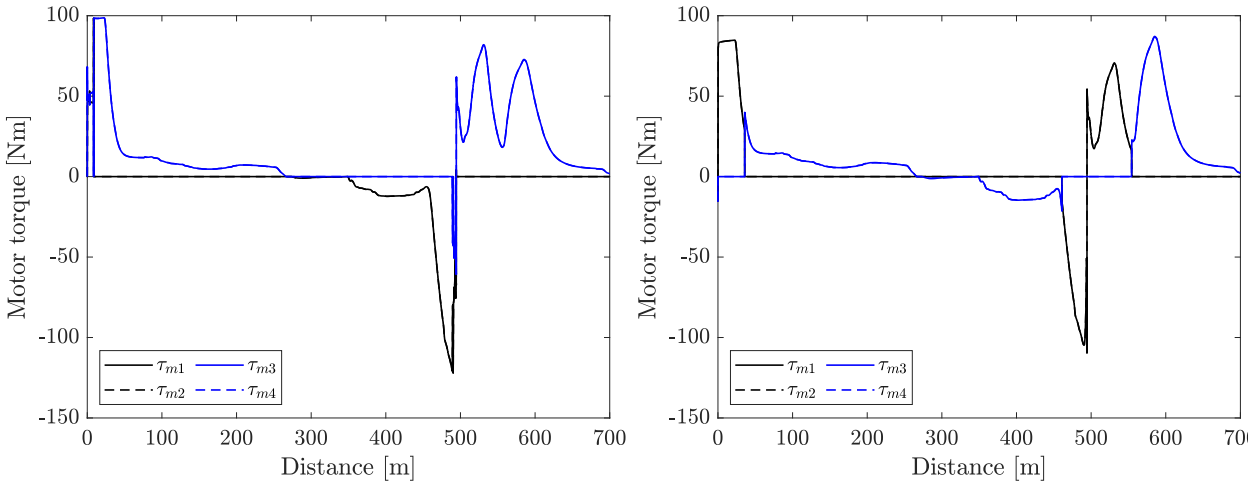

(a) *12/12* **(b)** *14/10*

Figure 4.4: *The effect of varying transmission ratio (front ratio/rear ratio) on torque distribution.*

the rear. The opposite, however, is not as energy efficient.

4.3 Energy consumption

The energy consumption from Paper I is presented in table 4.1. Both optimization methods perform similarly and decrease the energy consumption by 3.9%. When using QP without the ability to decouple the motors (QP w.o. coupling), the energy consumption is reduced by 0.2% which is relatively small compared to the case where there are couplings present. One can thus conclude that the majority of the total power loss origins from the motors, and hence the greatest energy saving potential lies in the ability to decouple the motors from the wheels.

As was seen in section 3.1.2 describing the driving scenario, it was concluded that the driving pattern of GCC and the driver model represented a moderate driver in an everyday drive cycle. Moderate driving does not induce a lot of longitudinal and lateral tire slips that give rise to slip power losses. It can thus be expected that the main energy saving potential lies in the motors.

Table 4.1: *Energy consumption GCC - longitudinal control from Paper I*

Strategy	[MJ]	Savings
ED	44.2	ref
Lookup	42.4	3.9%
QP w. coupling	42.4	3.9%
QP w.o. coupling	44.1	0.2%

In Paper II, a different transmission ratio is used than in Paper I as a result of the transmission study. The results are presented in table 4.2. The control allocator enables energy consumption to be reduced by 6% compared to equal distribution, and by 7.4% when the transmission ratio is optimized in combination with the control allocator.

Table 4.2: *Energy consumption GCC - longitudinal, lateral and yaw control from Paper II*

Strategy	n_f/n_r	[MJ]	Savings
ED	12/12	44.0	ref
QP w.o. coupling	12/12	43.9	0.3%
QP w. coupling	12/12	41.4	6.0%
QP w. coupling	14/10	40.7	7.4%

As discussed in section 4.1.2 there is little to no difference in lateral force distribution between the control allocator and reference. Hence, there is only optimization of torque distribution for the longitudinal force request. The difference in energy saving potential between the results presented in table 4.1 and 4.2 largely originates from the difference in transmission ratio. Again, the largest impact on energy consumption lies in the ability to decouple the motors.

Chapter 5

Conclusions & Future Outlook

In this final chapter, the two research questions posed in section 1.2 will be answered based on the results presented in chapter 4. A summary of the development steps taken in this thesis and their effect on the reduction in energy consumption in chosen drive cycle can be seen in figure 5.1. The reference for each development step is equal torque distribution with a transmission ratio of 10 in the front and rear. The chapter is finalized by recommendations on future research will be presented in section 5.2.

5.1 Conclusions

I. How to allocate individual wheel or axle-wise drive and brake torques to minimize power loss and at the same time follow the driver intentions on vehicle motion?

Two optimization based control allocation algorithms have been developed using a hierarchical control architecture. Driver inputs are translated through a reference generator that outputs planar vehicle force and torque requests that enter the control allocator. The control allocator distributes wheel torque and front wheel steering angle based on an optimization problem with the objective to minimize power losses in the electric drivetrain and tires. Two control allocation algorithms were developed using offline and online optimization methods. The algorithms were kept as simple as possible in order to facilitate implementation in a real vehicle.

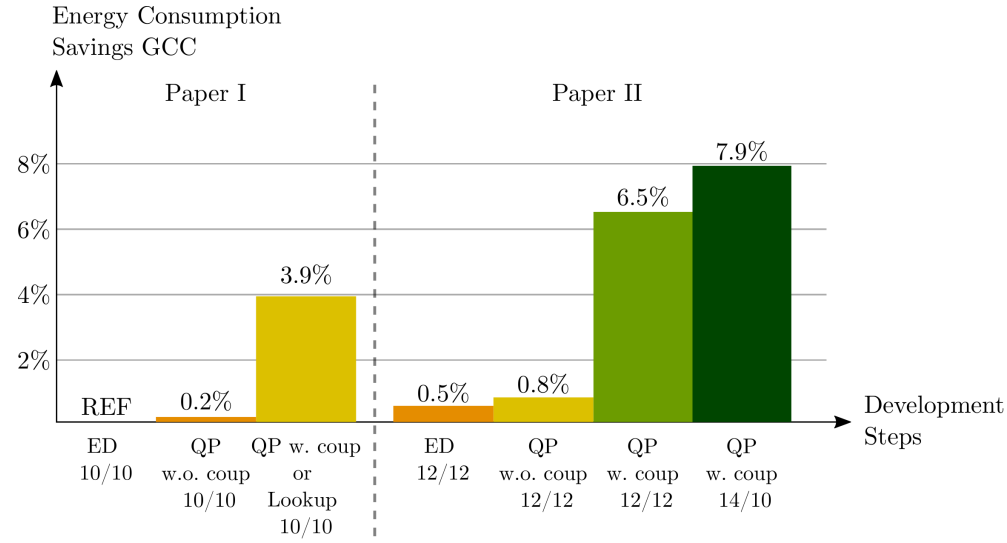

Figure 5.1: *Summary of the development steps in present thesis and their effect on energy consumption.*

The lookup table resulting from the offline optimization is easy to implement in a real vehicle and only requires information about current vehicle speed and longitudinal force request. It is, thus, a simple and efficient method. However, the inclusion of other types of actuators (apart from the electric motors used in this thesis) such as front and rear steering angles, and additional planar motion requests such as $F_{y,req}$ and $M_{z,req}$, the dimension of the lookup table increases and it quickly becomes complex. Furthermore, in order to include different operating conditions such as varying normal load and road friction, the number of lookup tables needed increases. In this thesis, it was used when optimizing wheel forces in the longitudinal direction.

In contrast, the control allocation algorithm using online optimization in the form of a quadratic program is more flexible to different types of actuators and an increasing number of planar motion requests in the sense that the changes are made in the control effectiveness matrix $\mathbf{B}$, the virtual control input $\mathbf{v}$ and control variables $\mathbf{u}$. The control allocation algorithm is more easily scalable as opposed to a lookup table, and can include functions of operating conditions. The optimization problem is convex provided a convex set of constraints which means that it will always find a solution, and since the problem is convex, every local minimum is a global minimum.

An analytical approach is used where the solution to the optimization problem is found through matrix operations. Hence, the solution is provided fast since no iterations are required. The quadratic program was used for optimization of wheel forces in the longitudinal direction only, and then in longitudinal, lateral and yaw direction combined.

Both control allocation algorithms contribute to a reduction in energy consumption. When the longitudinal motion is controlled, up to 3.9% energy can be saved in an everyday city cycle using either of the two algorithms. As can be seen in figure 5.1, the greatest energy saving potential lies in the ability to decouple either the front or rear motors. It was seen that in the chosen vehicle configuration the rear motors are used for low propulsion torque demands, the front motors are used for low brake torque demands and all four motors are used for high torque demands on either side of the spectrum. The motors that are not used are decoupled from the wheel.

II. In a vehicle with at least one electric machine on each axle, can different transmission ratios front and rear be used to reduce energy consumption?

In figure 5.1, it can be seen that by optimizing the transmission ratio for the equal wheel torque distribution strategy, the energy consumption was reduced by 0.5%. Using the control allocation algorithm QP without couplings, and additional 0.3%-units of energy could be saved. The largest energy saving potential however is the ability to decouple the motors, which reduces the energy consumption further by 5.7%-units. The same conclusion was drawn in Paper I. By finding the most optimal transmission ratio in combination with the control allocation algorithm QP with couplings, 1.4%-units of energy can be saved. It can be concluded that different transmission ratios front and rear, provided that the motors can be decoupled in present vehicle configuration, has a clear potential in reducing the energy consumption. By finding the optimal transmission ratio and using in combination with the control allocation algorithm QP with couplings, up to 7.9% can be saved compared to the original vehicle with transmission ratio 10 in the front and rear. Worth noting here is that the transmission ratio combination is optimized for the current drive cycle GCC, which does not imply that this transmission ratio is the optimal for all driving scenarios. In another drive cycle, the result might be different. Another interesting aspect revealed by figure 5.1 is that the greatest energy saving potential is enabled by a com-

bination of hardware and software. For example, the couplings belong to hardware but the decision on when to decouple either front or rear motors are decided by the control allocation algorithm, i.e. software. The optimization of transmission ratio was performed in combination with the control allocation algorithm, hence both hardware and software contribute to the reduction in energy consumption.

5.2 Future Outlook

The majority of the reduction in energy consumption, origins from the decoupling of the motors not in use, thereby avoiding power losses at zero torque. The permanent magnet synchronous machines (PMSM) used here are generally more efficient than asynchronous electric machines but suffers from power losses at zero torque due to a constant magnetic field (permanent magnets) in the motor. Asynchronous machines does not have this power loss as the magnetic field is not constant but generated by an electric current. Thus, a combination of different motor types could yield more energy efficient solutions. For example, the vehicle manufacturer Tesla has employed this strategy with an asynchronous motor used for low speed and high torque, i.e. start/stop situations, and a permanent magnet synchronous machine used at high speed and low torque, i.e. highway driving. According to [22], Tesla states that this results in an increase in efficiency by over 10%. However, whether a part of this percentage origins from replacing one of the two asynchronous machines with a more efficient PMSM is not clear. Future research includes the investigation of how combinations of different types of motors and motor sizes affect energy consumption.

The assumption of moderate driving during the development of the control allocation algorithms allows for many simplifications. Moderate driving implies that the driver request on vehicle planar motion can be fulfilled. The focus in this thesis has thus been on how to distribute torque and wheel angles based on energy efficiency. In more dynamic maneuvers, a trade-off will need to be made. In which situations it is acceptable to prioritize energy efficient solutions over driving dynamics need to be investigated in the future. For example, a fast torque distribution mode switch may induce oscillations in the drivetrain leading to jerk that may be unpleasant for the occupants in the vehicle. If the mode switch is performed in a curve it might

induce instability due to the effect of combined slip. Under the assumption of moderate driving, occurrences where there are high longitudinal and lateral accelerations simultaneously rarely occurs.

Furthermore, the assumption that 100% regenerative braking is possible is a question of system safety. For safety critical maneuvers the electric motors might not be able to handle the high request for brake torque. Thus, the integration of friction brakes in the architecture is necessary. This also applies to other safety critical functions such as electronic stability control and roll over stability. How to integrate these in the architecture and how they should communicate with the control allocator is a future topic to investigate.

Furthermore, a strong motivation for using control allocation in over-actuated systems is the ability to handle actuator failure and saturation. Complete actuator saturation, i.e. saturation on all actuators, has not occurred in the use case handled in this thesis, but will become more important in more dynamic maneuvers with higher longitudinal and lateral accelerations.

The lateral degree of freedom can be controlled by the inclusion of wheel steering angles as control variables. The use of a front wheel steered reference model will however limit the solutions to be front wheel steered due to that the lateral force and yaw torque request are coupled. In this case, the energy efficiency question is moved from the control allocator to the reference model. Future research should include how to find an energy efficient reference model, or how to design a reference model which places a request on vehicle position and heading angle based on driver input rather than planar vehicle forces.

The linearization of the planar equations of motion to fit intro the linear control allocation problem $\mathbf{Bu} = \mathbf{v}$ is appropriate when considering the longitudinal direction. It is also appropriate when including the lateral and yaw direction if combined slip is neglected. In order to include non-linear relations between control variables such as combined slip and steering effects on longitudinal force, this linearization is no longer sufficient. Non-linear constraints in the optimization problem will require non-linear programming which is computationally more demanding than the methods used in this thesis, making it harder to implement in a real vehicle. Future research should

include the development of a control allocation algorithm using non-linear programming that is accepted from a system safety perspective and real-time implementable. The integration of the control allocator with predictive energy management is also a topic for future research. Furthermore, steering of the wheel angles will lead to power losses in the motor belonging to the electronic power assist steering (EPAS) system. This needs to be taken into consideration during the minimization of power losses in the control allocator in the future.

Finally, the chosen power losses to be minimized here were in the electric drivetrain and in the tires. Validation of these power losses along with the control allocation algorithms will be performed in a real vehicle in the future.

Bibliography

[1] Y. Chen, J. Wang, *Energy-Efficient Control Allocation with Applications on Planar Motion Control of Electric Ground Vehicles*, American Control Conference, 2011.

[2] S. Torabi, M. Wahde, *Fuel Consumption Optimization of Heavy-Duty Vehicles Using Genetic Algorithms*, IEEE Congress on Evolutionary Computation, CEC 2017 - Proceesings, pp. 29-36, 2017.

[3] M. Henzler, M. Buchholz, K. Dietmayer, *Online velocity trajectory planning for manual energy efficient driving of heavy duty vehicles using model predictive control*, 17th International IEEE Conference on Intelligent Transportation Systems (ITSC), 2014.

[4] O. Härkegård., *Backstepping and Control Allocation with Applications to Flight Control*, Linköping Studies and Science and Technology, Dissertations No. 820, 2003.

[5] W. Durham, K.A. Bordignon, R. Beck, *Aircraft Control Allocation*, John Wiley & Sons, Ltd, 2017.

[6] T.A. Johansen and T.I. Fossen, *Control allocation - A survey*, Automatica 49 (2013), pp. 1087–1103.

[7] M. Bodson, *Evaluation of optimization methods for control allocation*, AIAA Guidance, Navigation, and Control Conference and Exhibit, 2001.

[8] L. Laine, J. Fredriksson, *Coordination of Vehicle Motion and Energy Management Control Systems for Wheel Motor Driven Vehicles.*, IEEE Intelligent Vehicles Symposium (IV'07), June, 2007.

[9] X. Zhang, D. Göhlich, *Optimal Torque Distribution Strategy for a Four Motorized Wheels Electric Vehicle*, International Electric Vehicle Symposium and Exhibition, EVS28, May 2015.

[10] A. Pennycott, L. De Novellis, A. Sorniotti, P. Gruber, *The Application of Control and Wheel Torque Allocation Techniques to Driving Modes for Fully Electric Vehicles*, SAE Int. J. Passeng. Cars - Mech. Syst., 7(2), 2014.

[11] A.M. Dizqah, B. Lenzo, A. Sorniotti, P. Gruber, S. Fallah, J. De Smet, *A Fast and Parametric Torque Distribution Strategy for Four-Wheel-Drive Energy-Efficient Electric Vehicles*, IEEE Transactions on Industrial Electronics, Vol.63, No.7, pp. 4367-4376, July 2016.

[12] B. Lenzo, G. De Filippis, A. Sorniotti, P. Gruber, S. Fallah, W. De Nijs, *Torque Distribution Strategies for Energy-Efficient Electric Vehicles With Multiple Drivetrains*, Journal of Dynamic Systems, Measurement, and Control, Vol.139, Dec. 2017.

[13] Y. Chen, J. Wang, *Energy-Efficient Control Allocation for Over-Actuated Systems with Electric Vehicle Applications*, Proceedings of the ASME 2010 Dynamic Systems and Control Conference, September 2010.

[14] Y. Chen, J. Wang, *Adaptive Energy-Efficient Control Allocation for Planar Motion Control of Over-Actuated Electric Ground Vehicles*, IEEE Transactions on Control Systems Technology, Vol. 22, No. 4, July 2014.

[15] M. Kissai, B. Monsuez, A. Tapus, *Review of Integrated Vehicle Dynamics Control Architectures*, European Conference on Mobile Robots, ECMR, 2017.

[16] L. Laine, *Reconfigurable Motion Control Systems for Over-Actuated Road Vehicles.* Doctoral Thesis, Chalmers University of Technology, ISBN 978-91-7291-960-0, 2007.

[17] A. Widyotriatmo, A.K. Pamosoaji, K-S. Hong, *Control Architecture of an Autonomous Material Handling Vehicle*, International Journal of Artificial Intelligence, Volume 10, Number S13, 2013.

[18] A.R. Girard, J.B. de Sousa, J.A. Misener, J.K. Hedrick, *A Control Architecture for Integrated Cooperative Cruise Control and Collision Warning Systems*, Proceedings of the 40th IEEE Conference on Decision and Control, 2001.

[19] P. Sun, *Improving energy-efficiency of electric vehicles by over-actuation*, Doctoral Thesis, Royal Institute of Technology, ISBN 978-91-7873-494-8, 2020.

[20] K.N. Genikomsakis, G. Mitrentsis, *A computationally efficient simulation model for estimating energy consumption of electric vehicles in the context of route planning applications*, Transportation Research Part D 50, pp. 98-118, 2017.

[21] J. Edrén, M. Jonasson, J. Jerrelind, A. Stensson Trigell, L. Drugge, *Energy efficienct cornering using over-actuation*, Mechatronics No.59, pp. 69-81, 2019.

[22] Ars Technica, *Motor technology from Model 3 helps Tesla boost Model S range 10%*, [cited 2020 Nov 16]; available from: https://arstechnica.com/cars/2019/04/motor-technology-from-model-3-helps-tesla-boost-model-s-range-10/#from-model-3-helps-tesla-boost-model-s-range-10/.